JGS
Journal of the Geological Society

Research article

Published online December 7, 2016 https://doi.org/10.1144/jgs2016-075 | Vol. 174 | 2017 | pp. 301–317

A detrital record of the Nile River and its catchment

Laura Fielding[1], Yani Najman[1*], Ian Millar[2], Peter Butterworth[3], Sergio Ando[4], Marta Padoan[4], Dan Barfod[5] & Ben Kneller[6]

[1] Lancaster Environment Centre, Lancaster University, Lancaster LA1 4YQ, UK
[2] NIGL, British Geological Survey, Keyworth, Nottingham NG12 5GG, UK
[3] BP Egypt, 14 Road 252, Al Maadi, Cairo, Egypt
[4] DISAT, University of Milano-Bicocca, Piazza della Scienza, 4 20126 Milano, Italy
[5] SUERC, Rankine Ave, Scottish Enterprise Technology Park, East Kilbride, G75 0QF, UK
[6] University of Aberdeen, Aberdeen AB24 3FX, UK
*Correspondence: y.najman@lancs.ac.uk

Abstract: This research uses analyses from Nile catchment rivers, wadis, dunes and bedrocks to constrain the geological history of NE Africa and document influences on the composition of sediment reaching the Nile delta. Our data show evolution of the North African crust, highlighting phases in the development of the Arabian–Nubian Shield and amalgamation of Gondwana in Neoproterozoic times. The Saharan Metacraton and Congo Craton in Uganda have a common history of crustal growth, with new crust formation at 3.0 – 3.5 Ga, and crustal melting at *c.* 2.7 Ga. The Hammamat Formation of the Arabian–Nubian Shield is locally derived and has a maximum depositional age of 635 Ma. By contrast, Phanerozoic sedimentary rocks are derived from more distant sources. The fine-grained (mud) bulk signature of the modern Nile is dominated by input from the Ethiopian Highlands, transported by the Blue Nile and Atbara rivers. Detrital zircons in the Nile trunk are predominantly derived from Phanerozoic cover rocks. Most detritus from the upstream White Nile is trapped in the Sudd marshes and contributes little to the Nile trunk. Therefore, the White Nile downstream is dominated by locally derived Phanerozoic cover. The White Nile proximal to the Gezira Fan is influenced by the fan's Blue Nile signature.

Supplementary material: Sample information, analytical methods and data tables are available at https://doi.org/10.6084/m9.figshare.c.3569490

Received 21 June 2016; **revised** 26 August 2016; **accepted** 30 August 2016

Modern river sediments can be used to efficiently sample large areas of upstream crust to help understand a region's geological history (e.g. Iizuka *et al.* 2013). In this study, we use a range of provenance techniques, including U–Pb and Hf isotope analysis of zircon from river sands, and Sr–Nd–Hf tracer isotope analysis of river mud samples, to characterize the catchment of the modern Nile River. Our aims are to gain a broad overview of the geological evolution of NE Africa, and to constrain the influences on sediment composition to the Nile River and ultimately the Nile delta cone, an important depocentre for hydrocarbon reservoirs.

We report data for sand and mud samples from the Nile trunk, and its tributaries the Blue Nile, White Nile and Atbara, together with samples from dry wadis and aeolian dunes from the Red Sea Hills and Western Desert, which represent possible sources of detritus to the river (Fig. 1). We have also studied sedimentary rocks from the Red Sea Hills and Western Desert that have draped NE Africa since the latest Precambrian. These rocks, and the modern wadi sands and aeolian dune sands that partly overlie them, which we have also studied, represent an important source of detritus to the river. We present zircon U–Pb and Hf-isotope data for gneissic basement within the Saharan Metacraton, which is poorly documented. These analyses help to characterize the nature of the Archaean crust of North Africa.

The Nile River is the longest river in the world, extending for more than 6800 km, and draining an area of *c.* 3.3 million km^2. The present-day Nile is made up of three main tributaries, the Blue Nile, White Nile and Atbara (Fig. 1). The mean annual water discharge during times of peak flow is dominated by the Blue Nile (68%), followed by the White Nile (10%) and Atbara (22%) (Williams & Adamson 1982). Sediment supplied to the Nile trunk in Egypt is dominated by contributions from the Blue Nile (50 – 61%) and Atbara (30 – 42%) (Padoan *et al.* 2011). The vast majority of the White Nile sediment load is trapped in extensive swamps in South Sudan (the Sudd marshes), thus accounting for <3% of the total Nile trunk sediment budget (Garzanti *et al.* 2015).

The White Nile drains Archaean–Proterozoic rocks of the Congo Craton, and extends through Precambrian rocks of the Saharan Metacraton (Abdelsalam *et al.* 2002). In its terminal tract, the White Nile has an extremely low gradient owing to its positioning along the floor of an ancient lake that occupied its valley as long ago as 400 ka before present (Williams *et al.* 2003). The present flow regime of the White Nile was established in the late Pleistocene, at *c.* 15 ka, when northwards flow was reinitiated as a result of intensification of the summer monsoon and resulting overflow of Lakes Albert and Victoria (Talbot *et al.* 2000; Williams *et al.* 2003).

The Blue Nile and Atbara, together with its tributary the Tekeze, are sourced in the Ethiopian Highlands, where they drain Cenozoic flood basalts (e.g. Pik *et al.* 1998), Neoproterozoic Arabian–Nubian Shield basement rocks (e.g. Evuk *et al.* 2014; Johnson 2014) and Phanerozoic cover sequences (e.g. Gani *et al.* 2009). Uplift of the Ethiopian Highlands in the Oligocene may have led to the initiation of flow in the Blue Nile. However, there is no consensus in the published literature regarding the timing of initiation of such flow, as summarized below.

Proponents of Oligocene initiation of Nile River sediment supply from the Ethiopian plateau have used knick-point facies to infer a three-phase incision in the Ethiopian Highlands at 29 – 10, 10 – 6 and 6 Ma, which instigated erosion in the Tekeze, Atbara and Blue Nile catchments (Gani *et al.* 2007). Thermochronological studies using apatite and titanite He ages suggest that the elevated plateau physiography, which controls most of the present-day Nile hydrology, has existed since the Oligocene, *c.* 29 Ma (Pik *et al.* 2003). Researchers favouring a Nile drainage originating in the Late Miocene cite sparse remotely sensed radar data to argue for a

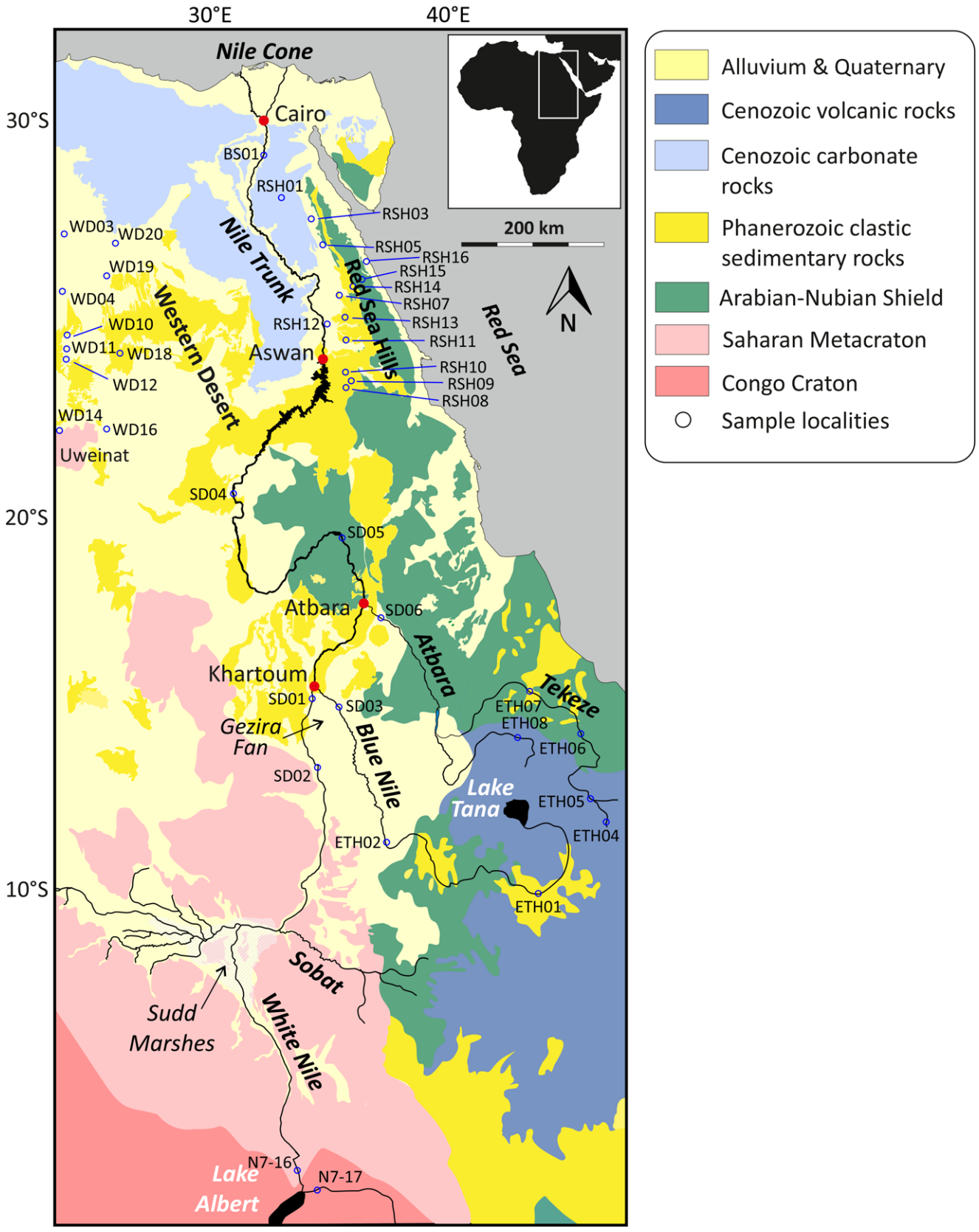

Fig. 1. Modern river samples and hinterland geology of Nile River source areas. Inset shows location of map as boxed area. Map modified from Kazmin (1972), al-Miṣrīyah (1981), Ministry of Energy and Mines (1981) and Johnson (2014).

south-draining 'Qena System' dominating the Nile valley until the Messinian Salinity Crisis (Issawi & McCauley 1992). Sediment volume calculations of the delta cone have been used to infer that a connection with the Ethiopian Highlands did not occur until the Pleistocene (Macgregor 2012; Palacios 2013).

The Red Sea Hills, to the east of the present-day Nile trunk, consist of Arabian–Nubian Shield basement and Phanerozoic sedimentary rocks that consist of Palaeozoic and Mesozoic clastic rocks and Eocene carbonates, partially overlain by modern wadi sands. Although not drained by the Nile at present, the Western

Desert, to the west of the present-day Nile trunk, is thought by Issawi & McCauley (1992) to have once contributed detritus to the main Nile trunk, and aeolian contribution occurs today (Garzanti *et al.* 2015). The Western Desert comprises reworked pre-Neoproterozoic crust of the Saharan Metacraton (Abdelsalam *et al.* 2002), and overlying Phanerozoic sedimentary successions. Modern-day wadi sediment and aeolian dunes currently cover a large proportion of both these regions.

Geology of the Nile catchment

The geology of east Africa has largely been shaped by the events of the Pan-African Orogeny when East and West Gondwana collided to form 'Greater Gondwana' at the end of the Neoproterozoic. The Pan-African Orogeny in NE Africa involved the collision of Archaean cratons such as the Congo Craton and the Saharan Metacraton with the Arabian–Nubian Shield, a terrane comprising Neoproterozoic, juvenile, oceanic island arcs. Phanerozoic cover sedimentary rocks blanket much of NE Africa, reflecting erosion from this mountain belt and subsequent Phanerozoic tectonics. The most prominent Phanerozoic tectonic events in the region involve rifting associated with opening of Neotethys, and later inversion associated with Africa–Mediterranean convergence. Uplift of the Ethiopian Highlands and surrounding area, and the eruption of continental flood basalts, is thought to have had a strong influence on the hydrology of this area in the Cenozoic.

Palaeoproterozoic and Archaean cratons

The cratons of Central Africa are formed of various blocks of Archaean and Palaeoproterozoic crust, flanked or truncated by Palaeoproterozoic to Mesoproterozoic orogenic belts. Together, these form the Congo Craton, defined as the 'amalgamated central African landmass at the time of Gondwana assembly' (De Waele *et al.* 2008). The Congo Craton (Fig. 1) forms part of the West African Central Belt, which formed at 2.0–3.0 Ga and comprises orthogneiss, metasediments and granitoids of the Tanzania Craton, Gabon–Cameroon Shield, Bomu–Kibalian Shield, Kasai Shield and Angolan Shield (Cahen *et al.* 1984; Walraven & Rumvegeri 1993; Goodwin 1996; Tchameni *et al.* 2000; De Waele *et al.* 2008).

The term Saharan Metacraton refers to an area of pre-Neoproterozoic continental crust that has, in part, been highly remobilized during the Pan-African Orogeny (Abdelsalam *et al.* 2002). It extends from the Arabian–Nubian Shield in the east to the Tuareg Shield in the west and the Congo Craton in the south. More than 50% of the Saharan Metacraton is overlain by Phanerozoic sedimentary rocks and desert sands (Abdelsalam *et al.* 2011). The poor exposure of the region means that the Saharan Metacraton, and its relationship to adjacent blocks, is poorly understood. The southern boundary is not well defined, but is taken to be marked by the Oubanguides orogenic belt, which separates it from the Congo Craton (Abdelsalam *et al.* 2002). Little modern geochronology has been carried out on rocks of the Saharan Metacraton. Legacy Rb–Sr and U–Pb data quoted by Abdelsalam *et al.* (2002) indicate a range of late Archaean and Palaeoproterozoic protolith ages, with significant cratonic reworking and addition of new crust in the Neoproterozoic. Bea *et al.* (2011) reported sensitive high-resolution ion microprobe (SHRIMP) U–Pb zircon ages as old as 3.22 ± 0.04 Ga for gneisses in the Uweinat and Gebel Kamil regions of the Western Desert in southernmost Egypt.

The Arabian–Nubian Shield

The Arabian–Nubian Shield is a collage of Neoproterozoic (*c.* 870 – 670 Ma) continental margin and juvenile island arcs, cut by voluminous granitoid intrusions as young as latest Neoproterozoic, and overlain by younger sedimentary and volcanic basins (Stern & Hedge 1985; Stern 1994; Johnson & Woldehaimanot 2003; Kusky & Matsah 2003). Only minor outcrops of pre-Neoproterozoic crust are found. Formation of the Arabian–Nubian Shield began with the initiation of subduction and development of magmatic arcs at 870 Ma. Terrane amalgamation associated with closure of the Mozambique Ocean and amalgamation of East and West Gondwana took place between *c.* 780 and *c.* 600 Ma (Johnson & Woldehaimanot 2003). To the west of the Red Sea, the oldest arc terranes (>800 Ma) of the Arabian–Nubian shield occur in the south, in Ethiopia, Eritrea and Sudan (Johnson & Woldehaimanot 2003). Ophiolitic rocks of the Eastern Desert of Egypt range in age from 810 to 720 Ma (Ali *et al.* 2010), and are overlain by younger volcanic and sedimentary sequences (e.g. Breitkreuz *et al.* 2010).

Ediacaran alluvial sedimentary rocks of the Hammamat Formation overlie the Arabian–Nubian Shield basement in the Eastern Desert of Egypt. The Hammamat Formation clastic rocks comprise terrestrial conglomerates, sandstones and mudstones in the Red Sea Hills area, and have proposed correlatives overlying the Midyan Terrane in NW Saudi Arabia (Bezenjani *et al.* 2014). Previous workers, using a variety of approaches (e.g. maximum depositional age determined from detrital minerals, dating of cross-cutting igneous units), have proposed ages ranging from 630 to 583 Ma for these rocks in Egypt (Willis *et al.* 1988; Wilde & Youssef 2002; Bezenjani *et al.* 2014). The Hammamat Formation rocks' depositional environments, and their relationship to the Pan-African Orogeny is of some debate (e.g. Ries *et al.* 1983; Wilde & Youssef 2002; Abdeen & Greiling 2005; Eliwa *et al.* 2010; Johnson *et al.* 2011; Bezenjani *et al.* 2014); the sediments are arguably (as described in the above-cited studies and references therein) considered to be pre-collisional, syn-collisional or post-collisional, and either locally sourced and deposited in isolated basins, or of distant provenance deposited from a major fluvial system of continental proportions.

The Pan-African Orogeny

During the Pan-African Orogeny, the final closure of the Mozambique Ocean led to amalgamation of the Saharan Metacraton and Congo Craton with the Arabian–Nubian Shield and the formation of the 'Trans-Gondwanan Supermountains' in the region that now forms NE Africa (Squire *et al.* 2006; Meinhold *et al.* 2013). To the south, it has been proposed (Abdelsalam *et al.* 2002) that collision between the Saharan Metacraton and Congo Craton resulted in the formation of the Oubanguides orogenic belt or Central African Fold Belt.

Phanerozoic sedimentary rocks

Erosion of the Trans-Gondwanan mountain belt and subsequent recycling of the eroded detritus during later inversion tectonics associated with various plate movements resulted in the deposition of a thick cover of fluvial and marine sediments overlying the amalgamated terranes, from the Cambrian onwards. Sedimentation continued until Cenozoic times, influenced by periods of tectonism. The most important of these tectonic events is the Mesozoic opening of Neotethys and later the South Atlantic, which resulted in the development of rift basins in the region, with Late Cretaceous–Early Eocene inversion of such basins as a result of the convergence of the Mediterranean with the African margin (Klitzsch & Squyres 1990; Guiraud *et al.* 2005; Bosworth *et al.* 2008).

Previous studies of the cover sedimentary rocks in regions adjacent to the Nile catchment (i.e. Libya; Meinhold *et al.* 2011; Altumi *et al.* 2013), Jordan and Israel (Kolodner *et al.* 2006; Morag *et al.* 2011)) have put forward contrasting Phanerozoic palaeo-drainage models for these regions during deposition of the cover.

The textural and mineralogical maturity of the bulk of the cover, and the provenance of the sediments, has been ascribed to varying degrees of recycling, long-distance transport and/or intense chemical weathering. Particularly debated is the origin of the *c.* 1000 Ma zircon population, for which an obvious significant basement source in the Saharan Metacraton or Arabian–Nubian Shield has not been recognized (Kolodner *et al.* 2006; Meinhold *et al.* 2011).

Cenozoic uplift and flood basalts

Uplift of the Red Sea Hills associated with opening of the Red Sea rift, and uplift in Ethiopia associated with eruption of voluminous continental flood basalts, has had a major influence on Nile drainage.

Many studies have attempted to ascertain the timing of Red Sea Hills uplift, with researchers suggesting that uplift of rift shoulders began around 24 Ma (Bosworth *et al.* 2005), 25 – 30 Ma (Ghebreab 1998), <29 Ma (Kenea *et al.* 2001) and 34 Ma (Omar & Steckler 1995).

The continental flood basalts that dominate much of the Ethiopian Highlands are associated with East African rift-related magmatism and continental break-up (Ebinger 2005; Buck 2006). Pre-rift basaltic and silicic magmatism initiated around 31 Ma (Baker *et al.* 1996; Rochette *et al.* 1998; Ukstins *et al.* 2002). Magmatic upwelling resulted in the uplift, extensional stresses and faulting within what is now the Ethiopian Highlands.

The provenance signal of modern Nile River sediments

The provenance of sediments in the Nile River has previously been studied using heavy mineral distributions and petrography, Sr and Nd trace isotope studies, and U–Pb analysis of detrital zircons.

Sr and Nd ratios have proved useful when recording major changes in provenance along the course of the Nile River (Padoan *et al.* 2011; Garzanti *et al.* 2013). High $^{87}Sr/^{86}Sr$ ratios and low ε_{Nd} values in White Nile muds from Archaean cratonic sources contrast with lower $^{87}Sr/^{86}Sr$ and higher ε_{Nd} in the Sobat River, which receives most of its sediment load from the crystalline basement and Cenozoic volcanic rocks of the Ethiopian Highlands. Isotope signatures of the Blue Nile and Atbara rivers are dominated by Ethiopian volcanic detritus and show low $^{87}Sr/^{86}Sr$ ratios and higher ε_{Nd} values.

Heavy mineral analysis and petrography have also been used to characterize the signature of the Nile catchment area (Garzanti *et al.* 2006). The Blue Nile, Atbara and Tekeze rivers drain predominantly flood basalts and rhyolitic ignimbrites in their upper courses until they reach the Neoproterozoic amphibolite-facies basement of the Arabian–Nubian Shield, consisting of granitoid gneisses, staurolite-bearing schists and marbles (Tadesse *et al.* 2003), and Phanerozoic sedimentary rocks found in the pre-rift sedimentary succession of the Blue Nile Canyon. Despite both rivers draining similar lithologies in the Ethiopian Highlands, the Atbara contains significantly less quartz than the Blue Nile.

The Victoria Nile downstream of its Lake Victoria output carries feldspatho-quartzose sand, with feldspars derived from granitoid rocks exposed locally (Garzanti *et al.* 2006). Downstream of the Lake Albert outlet, Albert Nile sand is quartzose with few feldspars and poor heavy-mineral suites with epidote, hornblende, kyanite, rutile and zircon. Sediment composition changes across South Sudan, and White Nile sand of all grain sizes downstream of the Sudd marshes chiefly consists of monocrystalline quartz, becoming slightly enriched in plagioclase, volcanic lithic fragments and clinopyroxene when downstream of the Gezira Fan. This fan deposit is ultimately derived from the Ethiopian flood basalts via a Pleistocene overspill from the Blue Nile (Garzanti *et al.* 2006).

The Red Sea Hills lie adjacent to the Nile River through much of its course through Sudan and Egypt. However, Red Sea Hills derived sediment has not been considered as an end-member in modelling of the Sr and Nd isotope composition of sediments in the Nile delta cone (Krom *et al.* 2002; Revel *et al.* 2014). Although construction of the Aswan High Dam has clearly affected the trunk Nile sediment flux downstream, comparison of petrographic data from samples collected prior to and subsequent to construction of the dam indicates that sediment composition is minimally affected (Garzanti *et al.* 2015).

Iizuka *et al.* (2013) presented coupled U–Pb, Lu–Hf and O-isotope data for detrital zircons from a sample of modern Nile sand taken 'Near Cairo City'. They identified age peaks at 1.1 – 0.9, 0.85 – 0.7 and 0.7 – 0.55 Ga, with minor groups at *c.* 2.6 and 2.0 Ga. They noted that grains with ages between 0.85 and 0.7 Ga had positive ε_{Hf} values, and were likely to have been derived from juvenile crust in the Arabian–Nubian Shield. Zircons with ages of 1.1 – 0.9 and 0.7 – 0.55 Ga, coinciding with times of supercontinent assembly, showed wide variations in O-isotope composition and ε_{Hf}.

Be'eri-Shlevin *et al.* (2014) discussed U–Pb and Hf-isotope data for detrital zircons in Quaternary to Recent Israeli coastal sands, which are believed to have been derived by a combination of longshore drift and aeolian transport from the Nile delta. They concluded that the ubiquitous presence of 0.56 – 0.75 Ga detrital zircons with negative ε_{Hf} implies that the Arabian–Nubian Shield is not the main source of Nile sands. Rather, they believed that multiple recycling through Phanerozoic sedimentary rocks that blanketed North Africa explains the age and hafnium isotope composition of the detrital zircon populations, as well as the quartz budget of the system.

Analytical methods

Samples of medium sand and mud were taken from modern rivers, sedimentary bedrock and modern wadis and dunes. Sample locations are shown in Figure 1. A sample of gneissic basement was also collected from the Saharan Metacraton.

Zircon and rutile grains were separated using standard methods, then hand-picked and mounted in epoxy discs and polished to reveal their interiors. All zircon grains were imaged using cathodoluminescence (CL) prior to analysis. U–Pb analyses for both zircon and rutile were carried out at the NERC Isotope Geosciences Laboratory (NIGL), using a single-collector Nu-Attom mass spectrometer with one of three New Wave laser systems, typically using a 35 μm laser spot. Hafnium isotope composition of zircons was measured at NIGL using a Thermo-Electron Neptune Plus mass spectrometer, coupled to a New Wave 193UC or 193FX Excimer laser. A 50 μm spot was used, targeting previously dated zircon domains.

Plagioclase and white mica were separated from the light fraction remaining after zircon and rutile separation. $^{40}Ar/^{39}Ar$ analyses were carried out at SUERC, East Kilbride, using a GVi instruments ARGUS five-collector mass spectrometer using a variable sensitivity Faraday collector array in static collection (non-peak hopping) mode (Sparks *et al.* 2008; Mark *et al.* 2009).

Mud samples for Sr, Nd and Hf analysis were leached in 10% acetic acid to remove carbonate before spiking with ^{149}Sm–^{150}Nd, ^{176}Lu–^{180}Hf, ^{87}Rb and ^{84}Sr isotope tracers. Standard dissolution methods and ion-exchange chromatography were used to separate elements of interest. Sr and Nd isotope compositions were measured at NIGL on a Thermo-Electron Triton mass spectrometer using dynamic multi-collection. Hf isotope composition was analysed in static mode on a Thermo-Electron Neptune mass spectrometer coupled to a Cetac Aridus II desolvating nebulizer.

X-ray fluorescence major and trace element analysis was carried out at the Open University in Milton Keynes using standard methods. Pressed powder pellets were used for trace element measurements, and fused discs for major elements.

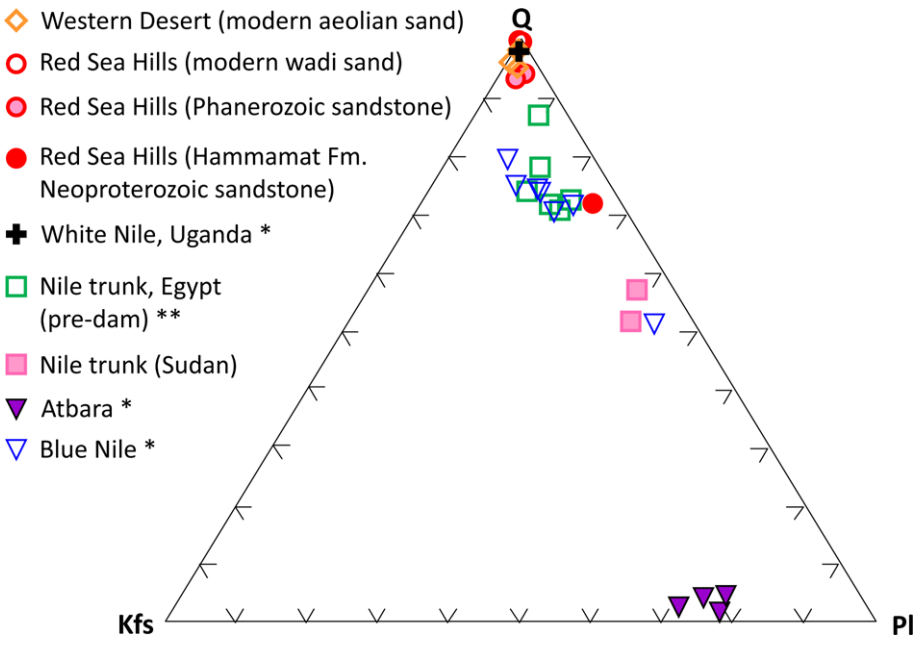

Fig. 2. Petrographic variability of detrital modes in modern river sands, bedrock and aeolian sands from the Nile trunk and hinterland, illustrating the proportion of quartz (Q), K-feldspar (Kfs) and plagioclase feldspar (Pl). Samples are modern river sands unless otherwise stated. *Data from Garzanti *et al.* (2006); **data from Garzanti *et al.* (2015).

Petrographic analysis and heavy mineral analysis of sands and muds were carried out at the Universita di Milano-Bicocca using methods modified from Garzanti *et al.* (2006) and Garzanti & Andò (2007). Assemblages were described in terms of transparent Heavy Mineral Concentrations (tHMC), Zircon–Tourmaline–Rutile Index (ZTR), Mineral Maturity Index (MMI) and Hornblende Colour Index (HCI).

Petrography and heavy mineral analysis

The analyses presented below are intended to provide data for regions that are not adequately covered by published datasets, summarized by Garzanti *et al.* (2015).

Red Sea Hills, Egypt

Modern wadi sands (RSH03A and RSH05A) in northern Egypt are sub-litharenites (Fig. 2), with carbonate clasts and minor chert and shale grains, and a poor to moderately poor tHMC of 1.2 ± 1.0. Epidote–amphibole–clinopyroxene transparent heavy mineral assemblages include minor garnet, zircon, rutile, staurolite and tourmaline (ZTR 10 ± 5). Phanerozoic sandstone samples (RSH08A and RSH09A) from the Red Sea Hills are quartz arenites with an extremely high ZTR of 98 – 99 and tHMC between 12 and 20. The modern wadi sands contain slightly more (4 – 5%) feldspar than the bedrock samples. This difference in mineralogical maturity between bedrock and wadi samples may reflect sampling bias as the modern wadi sands sample a larger area. By contrast, a sample from the Hammamat Formation (RSH14A) was found to be a sheared lithic–arkose volcaniclastic arenite dominated by epidote, with ZTR = 0 and tHMC = 73.

Western Desert, Egypt

Aeolian dune sands (WD03C, WD19C and WD20C) from the Egyptian desert west of the Nile are quartzose, with few feldspars (K-feldspar > plagioclase) and sedimentary rock fragments (limestone and subordinately siltstone–shale and chert). Very poor to moderately poor (tHMC of 0.8 ± 0.4) transparent heavy mineral assemblages include epidote, zircon, amphibole, rutile, tourmaline, clinopyroxene, staurolite, garnet, kyanite and titanite (HCI = 11 ± 1, MMI = 50, ZTR = 34 ± 13).

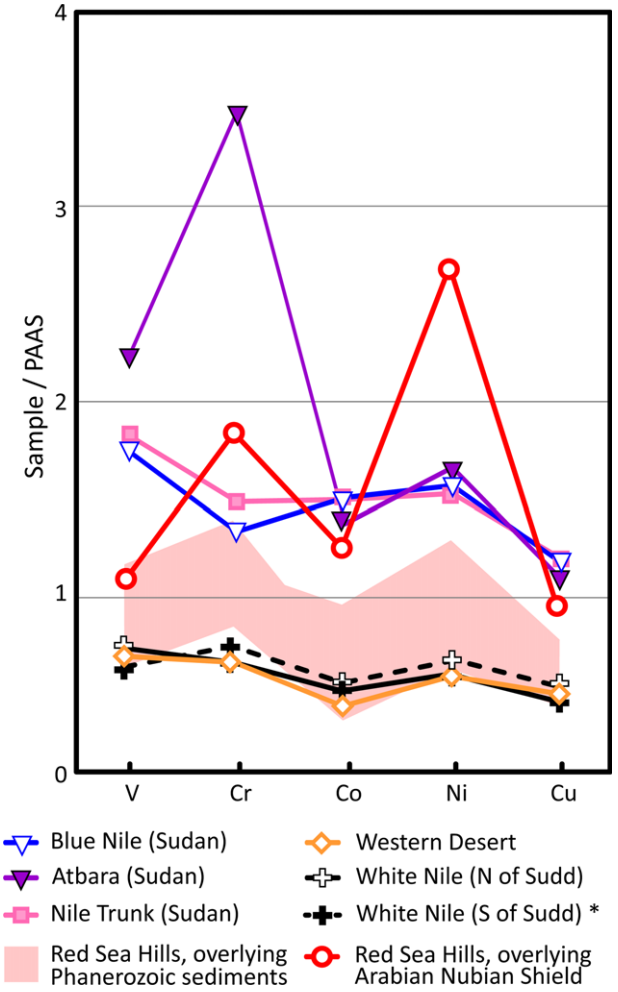

Fig. 3. Selected trace element concentrations from each of the Nile source areas and the main Nile trunk, normalized to trace element concentrations of Post-Archaean Australian Shale (PAAS: McLennan & Taylor 1985). All samples are modern muds or mudstones, except for samples from the Nile trunk in Egypt collected prior to construction of the Aswan Dam (Shukri 1949), which are modern sands. *Data from Garzanti *et al.* (2013). The field for Red Sea Hills samples encompasses 11 samples. Other distributions represent single analyses, or averages of small groups of samples.

Nile trunk, Sudan

Downstream of the confluence of the Blue Nile, White Nile and Atbara, sediments (SD04A and SD05A) are quartz-dominated with plagioclase feldspar more abundant than K-feldspar, and some volcanic detritus present. Both samples were found to be rich in transparent heavy mineral assemblages (tHMC of 16.8 and 10.1) including clinopyroxene, epidote and hornblende (HCl = 6 – 7). The ZTR for both Nile trunk samples was very low (0 – 1).

Major and trace element chemistry

Trace element results are presented in Figure 3, normalized to the trace element concentrations of Post-Archaean Australian Shale (PAAS), compiled by McLennan & Taylor (1985). V, Cr, Co, Ni and Cu concentrations allow us to determine the relative amount and location of mafic material within the Nile catchment area.

Values of V, Cr, Co, Ni and Cu are considerably higher in the Blue Nile and Atbara rivers than in the White Nile, reflecting the significant proportion of continental flood basalts in the Blue Nile and Atbara catchments. Similarity between the Blue Nile–Atbara values and those of the Nile trunk in Sudan attest to the dominance of the Blue Nile–Atbara contribution compared with the White Nile to the trunk river downstream.

Western Desert values are similar to the White Nile values, reflecting their location in proximity to cratonic rocks. Red Sea Hills values show a greater mafic influence owing to their closer proximity to the Arabian–Nubian Shield. Of note is the difference between Red Sea Hills wadi muds collected from locations overlying Red Sea Hills Phanerozoic bedrock and Red Sea Hills wadi muds from locations directly overlying Arabian–Nubian Shield basement (samples RSH14B and RSH15B). The Ni spike in the latter most probably reflects significant derivation from the underlying ophiolitic ultramafic rocks of the Arabian–Nubian Shield.

Zircon U–Pb geochronology and Hf isotope signatures

Zircon U–Pb and hafnium isotope data are shown in Figures 4 – 8. The locations of all analysed samples are shown in Figure 1.

Cratonic sources

Western Desert Archaean gneiss

The oldest bedrock sample analysed (WD16A) is a gneiss, mapped as Archaean crust of the Saharan Metacraton (Daumain *et al.* 1958), collected east of Uweinat in southernmost Egypt. Zircon crystals have oscillatory-zoned cores under CL, with homogeneous CL-dark, possibly metamorphic overgrowths (Fig. 4 inset). Cores are commonly broken, with abrupt terminations, suggesting that the sample may have had a sedimentary protolith that has undergone high-grade metamorphism.

Fifteen U–Pb analyses of zircon cores have $^{207}Pb/^{206}Pb$ ages ranging from 2924 to 3235 Ma, with a single analysis giving a statistically younger age of 2794 Ma. It is not possible to identify statistically valid populations within the zircon core dataset owing to the small number of cores and rims found in the samples. This may reflect a detrital source for the zircons. The zircon cores have an average ε_{Hf} of −2.3, and a weighted average depleted mantle model age (TDM_{Hf}) of 3479 ± 47 Ma (MSWD = 4.1, n = 15/16).

Five analyses of zircon rims form a cluster with a weighted average $^{207}Pb/^{206}Pb$ age of 2701 ± 32 Ma. Three further rim analyses yield younger $^{207}Pb/^{206}Pb$ ages, between 2524 and 2587 Ma. The zircon rims yield an average ε_{Hf} of −10.6 and a weighted average TDM_{Hf} of 3467 ± 45 Ma (MSWD = 2.2, n = 8), within error of the age derived from zircon cores, indicating that new zircon growth took place in a closed system during high-grade metamorphism (Flowerdew *et al.* 2006). The weighted average model age of all zircon analyses in this sample is 3474 ± 31 Ma (MSWD = 3.3, n = 23/24). It is notable that the Th/U ratio of cores (0.37 – 1.3) is considerably higher than that in the rims (0.03 – 0.14), supporting a metamorphic origin for the rims.

White Nile (Uganda)

Modern river sands were collected from the White Nile upstream of the Sudd marshes at Wadelai (N7-16S) and Murchison Falls (N7-17S) in northern Uganda. Both samples show a similar distribution of Archaean ages, with maxima at *c.* 2620 Ma (Fig. 5), and only a few older grains. Analyses with $^{207}Pb/^{206}Pb$ ages of 2500 – 2570 Ma commonly occur as

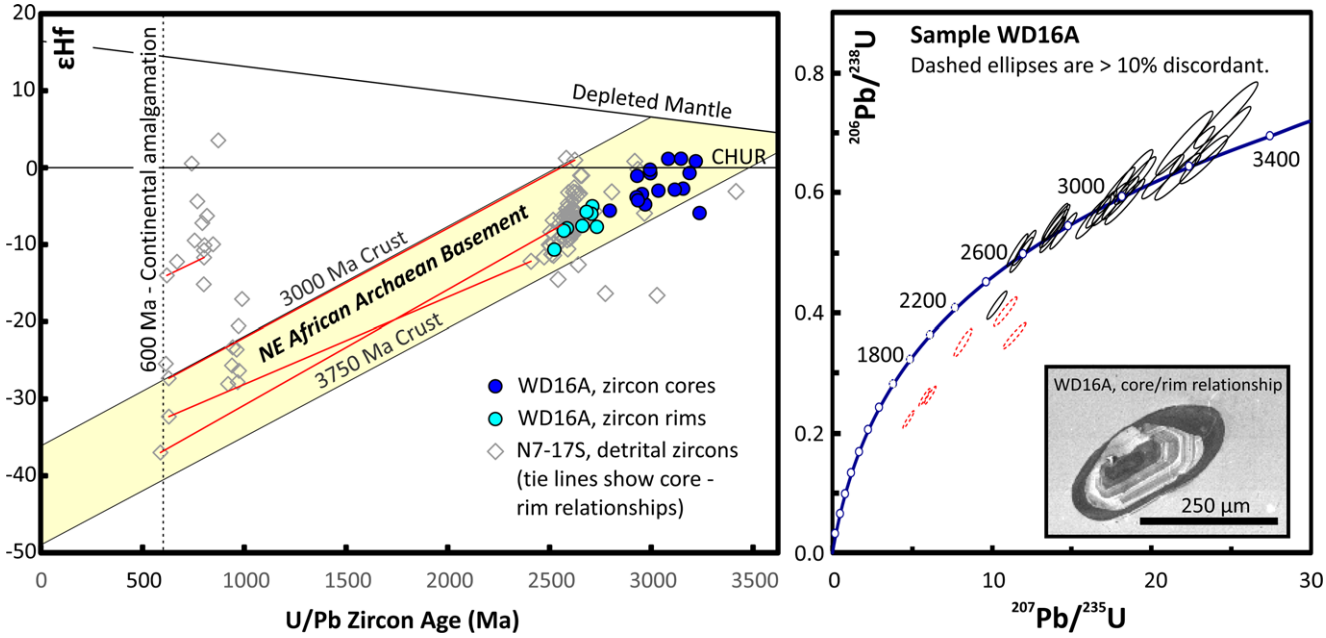

Fig. 4. U/Pb age and hafnium isotope composition of complex zircons in Archaean gneiss within the Saharan Metacraton (WD16A), and detrital zircons in White Nile sand draining Archaean craton (N7-17S). Two-sigma uncertainties are smaller than the symbol size, typically *c.* 20 Ma on the age determinations, and 1 – 2 ε_{Hf} units.

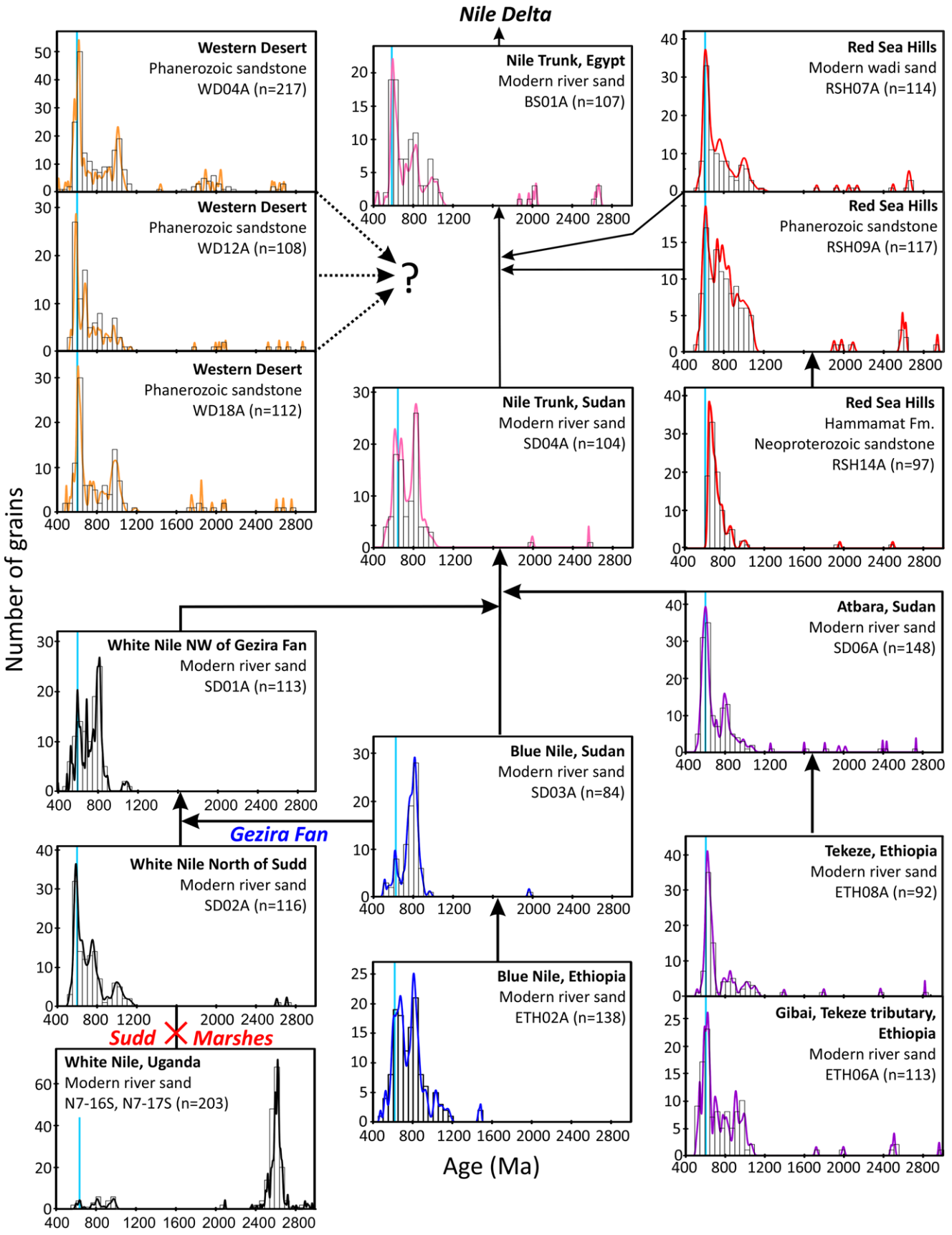

Fig. 5. Detrital zircon U–Pb age frequency and relative probability plots for samples from the Nile catchment and surrounds.

overgrowths on older zircon cores. Only 3% of grains in sample N7-16S give younger, Neoproterozoic to Mesoproterozoic ages. However, sample N7-17S contains 24% of such grains, with significant populations at *c.* 630, 800 and 900 – 1000 Ma.

The *c.* 2620 Ma zircon population in sample N7-17S typically shows oscillatory zoning under CL, and has an average ε_{Hf} of −7 and a TDM_{Hf} of 3412 ± 23 Ma (MSWD = 2.3, *n* = 68/74; Figs 4 and 6). Eight grains with ages between 900 and 1000 Ma have an

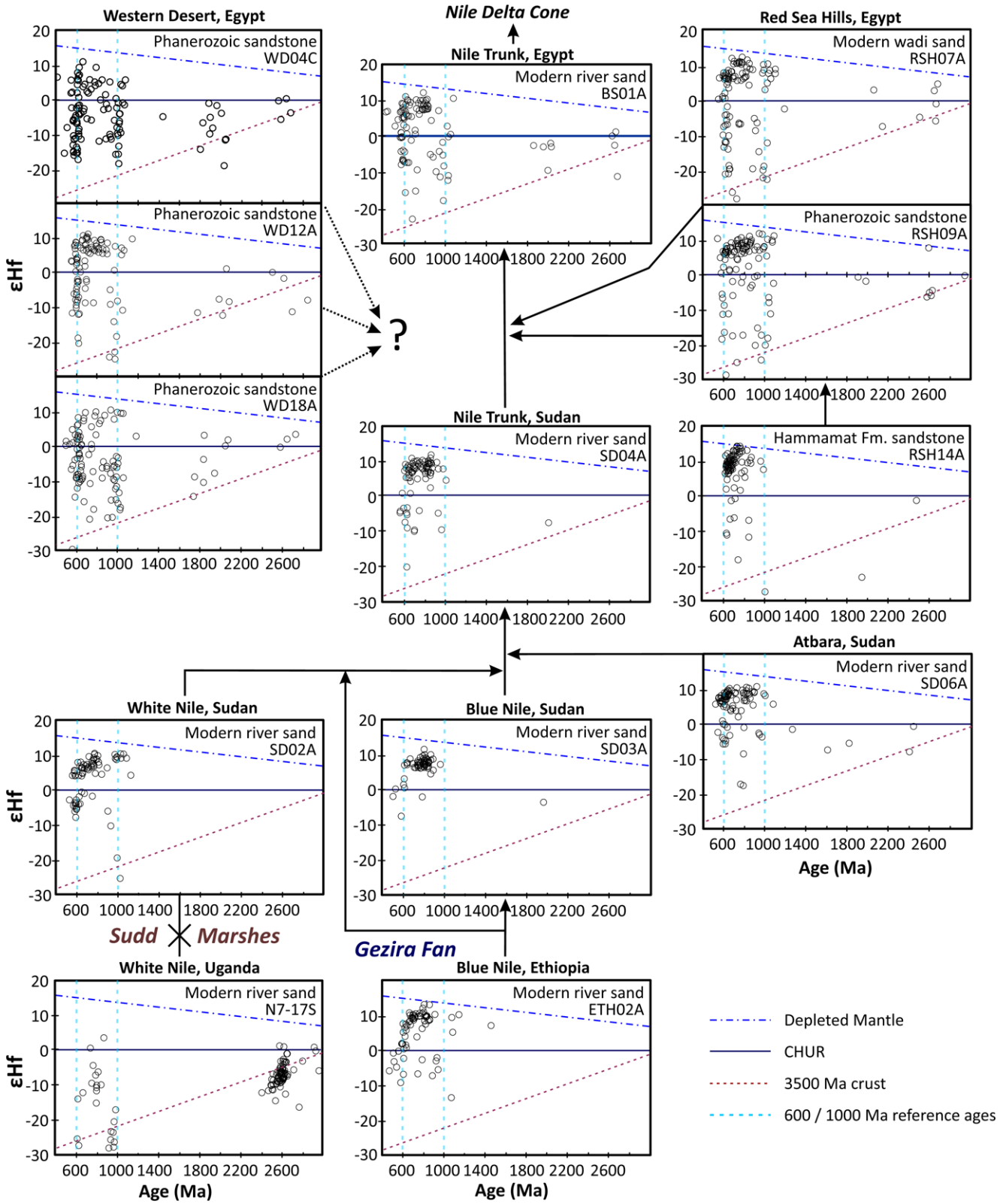

Fig. 6. Detrital zircon U–Pb age frequency and relative probability plots with ε_{Hf} v. U–Pb age. The vertical line at 600 Ma marks the approximate time of the Pan-African Orogeny and the collision of the Arabian–Nubian Shield with the Saharan Metacraton and Congo Craton. The vertical line at 1000 Ma highlights the dual juvenile and cratonic populations of the enigmatic 1000 Ma population. The reference line for 3500 Ma crust is calculated using $^{176}Lu/^{177}Hf$ ratio of 0.017, which is derived from the apparent crustal evolution trend displayed in Figure 4.

average ε_{Hf} value of −24, a composition that is consistent with formation by melting of Archaean crust similar to that represented by the *c.* 2620 Ma zircon population. The 900 – 1000 Ma grains show oscillatory zoning with no evidence for core–rim relationships. Zircons with ages between 670 and 870 Ma have ε_{Hf} between +3.5 and −15, requiring input of juvenile material in addition to Archaean crust. These grains are typically CL-light, and weakly zoned or unzoned, with Th/U of 0.22 – 0.89.

Four analyses of rims on Archaean zircon cores give ages of *c.* 630 Ma, with an average ε_{Hf} of −30.5 (Fig. 4). The overgrowths

show no zoning under CL, and have low Th/U (≤0.03), suggesting a possible metamorphic origin. A single zircon rim, which formed on a *c.* 800 Ma grain, also gives an age of *c.* 630 Ma, with $\varepsilon_{Hf} = -14$, again consistent with growth in a closed system under metamorphic conditions (Flowerdew *et al.* 2006).

Figure 4 includes a field for NE African Archaean Basement, which is derived using the composition of zircons in the Saharan Metacraton gneiss (WD16A) and the detrital zircon grains from the White Nile at Murchison Falls (N7-17S). The slope of the observed trend is consistent with an average $^{176}Lu/^{177}Hf$ ratio in the sampled North African crust of *c.* 0.012. This field represents the likely composition of craton-derived grains in other sedimentary rocks of the Nile catchment, discussed below.

Arabian–Nubian Shield cover; the Hammamat Formation

Sample RSH14A is a volcanic arenite collected within conglomerates of the Hammamat Formation, in Wadi Hammamat (El-Rahman *et al.* 2010). The Hammamat Formation in this area was folded and cleaved prior to intrusion of the Um Had granite at 596.3 ± 1.7 Ma (Andresen *et al.* 2009).

Sample RSH14A has a rich heavy mineral assemblage dominated by epidote. Zircon grains are dominated by *c.* 630 – 780 Ma grains with juvenile hafnium isotope values (Fig. 6). Eighty per cent of the overall zircon population have positive, juvenile ε_{Hf} values (Fig. 6). Grains in the region of 700 – 800 Ma show higher ε_{Hf} values (+14) than seen in any other sample in the Nile catchment area. Two per cent of analysed grains gave Palaeoproterozoic or Archaean ages.

Only four grains give apparent ages younger than 620 Ma, the youngest having a $^{206}Pb/^{238}U$ age of 596 ± 18 Ma, within error of the age of the structurally much later Um Had granite. The timing of deposition of the Hammamat Formation is unclear, with suggested ages ranging between 630 and 583 Ma (Willis *et al.* 1988; Wilde & Youssef 2002; Bezenjani *et al.* 2014). It is therefore critical to establish whether these young grains could be used to determine a maximum depositional age for the Hammamat Formation, or whether these grains may have been affected by Pb loss. Several grains with ages younger than 645 Ma were therefore revisited, and five new analyses were carried out on each grain. All grains yielded ages of *c.* 635 Ma or older, confirming that the original analyses had been affected by Pb loss (Fig. 7). The original analyses used a large laser spot size (35 μm, compared with 20 μm for the new analyses), which may have been more likely to intersect cracks and defects in the grains.

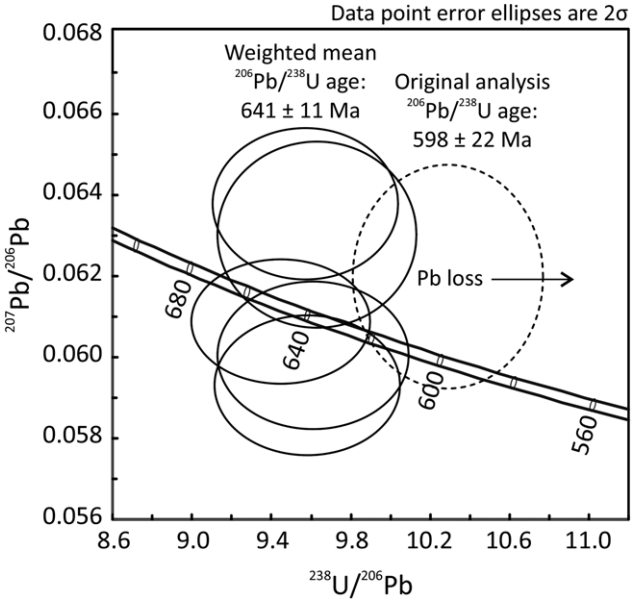

Fig. 7. Tera–Wasserburg plot illustrating the effect of Pb loss on an apparently 'young' Hammamat Formation zircon grain. Replicate analyses of the same grain indicate a true age *c.* 40 myr older.

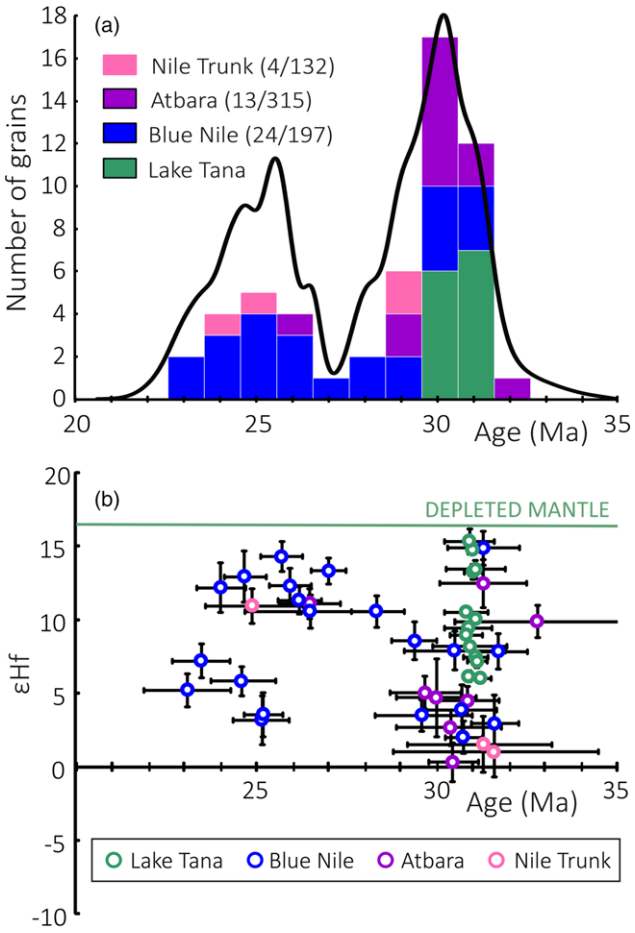

Fig. 8. Cenozoic zircon data from the modern Nile catchment. (**a**) Histograms for Cenozoic detrital zircons from the Nile and its tributaries, together with zircons from Lake Tana rhyolites from the Ethiopian Highlands (ages from Prave *et al.* 2016). Probability density plot is shown for combined data. (**b**) Plot of initial ε_{Hf} values against age for detrital zircons from the modern Nile and its tributaries, together with zircons from the Lake Tana rhyolites. Numbers in parentheses in the key indicate the number of Cenozoic grains detected in each sample relative to the total number of grains analysed. It should be noted that zero Cenozoic grains were recorded in the modern White Nile and Red Sea Hills modern wadi sediments.

Phanerozoic cover rocks

Western Desert (Egypt)

Samples WD04A, WD12A and WD18A (Figs 5 and 6) are Phanerozoic sandstones. These samples have a dominant zircon population at *c.* 600 Ma, with >60% of grains of this age showing negative ε_{Hf}. Zircons between 700 and 900 Ma are dominated by more juvenile grains, with positive ε_{Hf}. A population of *c.* 1000 Ma grains appears to fall into two distinct groups, with juvenile and more crust-dominated hafnium compositions. In addition, subordinate populations of Palaeoproterozoic and Archaean grains (totalling *c.* 10%) and sparse Phanerozoic grains are present.

Red Sea Hills (Egypt)

Sample RSH09A is a Phanerozoic sandstone from Wadi Kharit in the Red Sea Hills. Zircons are dominated by peaks at *c.* 620, 730 –

900 and 1000 Ma, with predominantly juvenile ε_{Hf}. A minority of grains at *c.* 620 and 1000 Ma show more cratonic ε_{Hf} values. Twenty-five per cent of *c.* 620 Ma grains and 42% of *c.* 1000 Ma grains show negative ε_{Hf}. Eight per cent of grains give Archaean or Palaeoproterozoic ages.

Modern wadi sands

Sample RSH07A is a modern wadi sand collected in Wadi Hammamat in the Red Sea Hills, deposited on Phanerozoic sandstone bedrock. The zircon age and ε_{Hf} isotope distribution are similar to those of the Red Sea Hills Phanerozoic bedrock sample, with peaks at *c.* 620, 770 and 1000 Ma. Fifty per cent of 620 Ma grains and 42% of *c.* 1000 Ma grains have cratonic ε_{Hf} values. Eight per cent of grains give Archaean or Palaeoproterozoic ages.

Modern river sands

Blue Nile

Sample ETH02A was collected from the Blue Nile Gorge in the Ethiopian Highlands. It shows two main zircon age populations at 660 – 720 and 800 – 850 Ma. ε_{Hf} values are dominantly juvenile, although sparse grains at 500 – 600 Ma yield ε_{Hf} values as low as −10. Sparse *c.* 1000 Ma ages are also present, but Archaean and Palaeoproterozoic ages are absent. Juvenile Cenozoic grains are present (Fig. 8). Sample SD03A was collected near Wad Madani in Sudan. It is dominated by 750 – 850 Ma zircons with juvenile ε_{Hf} values. Only sparse *c.* 600 Ma grains are found, and only one Palaeoproterozoic age was recorded.

Tekeze

Sample ETH06A was collected from the Gibai River, a tributary of the Tekeze, whereas sample ETH08A was collected further downstream at Malemin Bridge. Both samples show dominant peaks at *c.* 620 Ma and a number of peaks ranging back to *c.* 1000 Ma. Sparse Palaeoproterozoic and Archaean grains make up *c.* 6% of each population. A single Cenozoic grain was identified in each sample.

Atbara

Sample SD06A was collected from the Atbara close to its confluence with the Nile trunk in Sudan. The most dominant population forms a peak at *c.* 600 Ma, with a subordinate peak at *c.* 800 Ma, both dominated by juvenile ε_{Hf} values. Palaeoproterozoic and Archaean grains are sparse (3%). Cenozoic grains make up 6% of the population.

White Nile

Sample SD02A was collected from the White Nile downstream (north) of the Sudd marshes in Sudan, and south of the Gezira Fan. Zircons are dominated by *c.* 600 Ma grains, with subpopulations showing both juvenile and more cratonic ε_{Hf} values. Older age peaks at *c.* 850 and 1000 Ma are dominated by juvenile ε_{Hf} values. Only two Archaean grains were identified (*c.* 2%), in marked contrast to sample N7-17S (see above) from upstream (south) of the Sudd marshes.

Sample SD01A was collected downstream of the Blue Nile-sourced Gezira Fan. It shares similar peak characteristics to sample SD02A, but with more dominant *c.* 650 and 1000 Ma populations.

Nile trunk

Sample SD04A captures the signature of the Nile trunk in northern Sudan, downstream of the confluences of the Blue Nile, White Nile and Atbara, but upstream of the Aswan Dam. The detrital zircon age and ε_{Hf} distribution are similar to those of the upstream Blue Nile sample (ETH02A), with peaks at *c.* 630, 680 and 830 Ma, all dominated by juvenile ε_{Hf} values. Only two Archaean to Palaeoproterozoic ages are present (2%). Four Cenozoic ages were measured.

Sample BS01 was collected north of the Aswan Dam at Al Wasta, south of Cairo. It is dominated by *c.* 600 Ma zircons, with smaller populations at *c.* 830 and 1000 Ma. ε_{Hf} values show dominantly juvenile values, but 11% of *c.* 600 Ma and 73% of *c.* 1000 Ma grains have negative, craton-influenced values. Archaean and Palaeoproterozoic grains make up 9% of the zircon population. No Cenozoic grains were observed.

Ar/Ar mica and plagioclase feldspar and U/Pb rutile

Samples analysed include White Nile, Blue Nile and Atbara, Nile trunk, Red Sea Hills modern wadi and bedrock, and Western Desert aeolian samples.

The $^{40}Ar/^{39}Ar$ mica and plagioclase data and the U–Pb rutile data all show an overwhelming Pan-African signature (*c.* 600 Ma). This includes the White Nile samples upstream of the Sudd, despite having a strongly Archaean signature in U/Pb zircon analyses, and indicates strong overprinting by the Pan-African Orogeny in this region. The Blue Nile also contains Cenozoic feldspars, derived from the Ethiopian Highlands and in agreement with the presence of Cenozoic zircons also recorded in this river (see above).

Although the number of white mica analyses is small, we observe a change in signal between White Nile sands south of the Sudd marshes and the Nile trunk and Red Sea Hills to the north. The White Nile sample (N7-17S) is dominated by a single population with a mean age of *c.* 615 Ma. By contrast, both the Nile trunk in Sudan (Sample SD04A) and a Red Sea Hills wadi sand (RSH07A) show age peaks at *c.* 600 and 650 Ma.

Sr, Nd and Hf isotope bulk analysis

Bedrock mudstone, and mud samples from the surface of flash-flood deposits, were collected in the Red Sea Hills. The samples show a limited range in isotope composition (Figs 9 and 10), with moderately radiogenic $^{87}Sr/^{86}Sr$ (averaging 0.7096), and non-radiogenic ε_{Nd} (averaging −6.1) and ε_{Hf} (averaging −4.9). Mudstones, muds and aeolian sands were collected in the Western Desert. These show considerably more scattered results, with radiogenic $^{87}Sr/^{86}Sr$ (0.708 – 0.716) and non-radiogenic ε_{Nd} (−5.8 to −12.8) and ε_{Hf} (−8 to −21.6).

Modern river mud samples collected from the Atbara and Tekeze rivers have Sr, Nd and Hf isotope compositions similar to average Ethiopian basalts (Figs 9 and 10; Pik *et al.* 1999; Meshesha & Shinjo 2010). Samples from the Blue Nile and the Nile trunk in northern Sudan plot on trends towards higher $^{87}Sr/^{86}Sr$ and lower ε_{Nd} and ε_{Hf}, consistent with incorporation of older sediment derived from sources other than Ethiopian basalt. Average values for Holocene Nile trunk sediments in northern Sudan, and sand samples collected in Egypt before the construction of the Aswan High Dam, also plot on this trend (Shukri 1949; Woodward *et al.* 2015). A sample collected from the White Nile just south of its confluence with the Blue Nile at Khartoum plots close to the Nile trunk trend.

Three modern river mud samples have what, at first glance, appear to be anomalous isotope compositions, given their locations. A sample (ETH07B) from the Uri River, Ethiopia, a tributary of the Tekeze in Ethiopia, has values unlike those one might expect from the Ethiopian plateau continental flood basalt region. However, the Uri River's local catchment drainage basin geology is in fact Phanerozoic cover (Fig. 1), consistent with its isotopic signature. Samples SD01B and SD02B are White Nile samples, yet their Sr–Nd signatures are similar to those of the Blue Nile and Phanerozoic

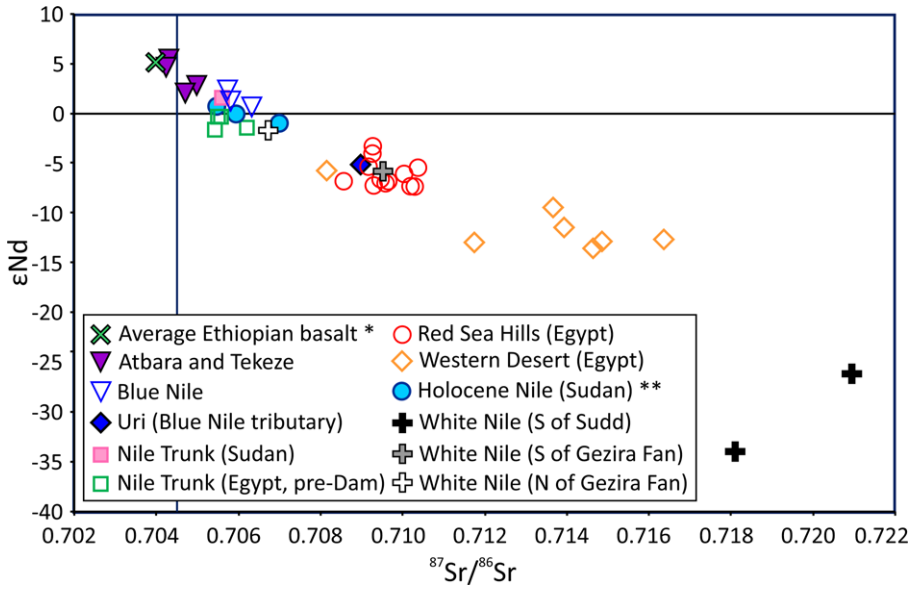

Fig. 9. $^{87}Sr/^{86}Sr$ v. ε_{Nd} isotope data for Nile river muds; Egyptian Nile trunk sands taken prior to the construction of the Aswan Dam (samples from Shukri 1949); Nile hinterland mudstones, wadi muds and aeolian sands; and Sudanese Holocene Nile trunk samples (Woodward *et al.* 2015). Also shown for comparison are average data from the Ethiopian Continental Flood Basalts (Pik *et al.* 1999).

cover respectively. This is consistent with, in the case of SD01B, its location downstream of the Gezira Fan, which is an overspill of Blue Nile detritus, and in the case of SD02B, its location downstream of the Sudd Marshes, which act as a sediment trap to the upstream White Nile, and thus its provenance is locally derived, as discussed in more detail in following sections.

Two samples collected from the Albert and Victoria branches of the Nile in Uganda were also analysed. These have highly radiogenic $^{87}Sr/^{86}Sr$ (0.718, 0.721), and non-radiogenic ε_{Nd} (−26.3, −34.1) and ε_{Hf} (−25.9, −55.4) consistent with derivation from local cratonic basement.

Excluding the three anomalous samples described above, for which local geological anomalies provide explanation, and the White Nile samples taken from Uganda, the range in isotope composition shown by the Nile and its tributaries is rather limited: $^{87}Sr/^{86}Sr$ varies from 0.7043 in the Atbara to 0.7067 in the White Nile sample from Khartoum, ε_{Nd} varies from 5.5 to −1.8, and ε_{Hf} varies from 10.8 to −1.8.

Discussion

Our data document early crust-forming events, Precambrian orogenies culminating in the Neoproterozoic assembly of Gondwana, subsequent erosion and deposition of voluminous sediments, and finally Cenozoic uplift of the Red Sea Hills and Ethiopian Highlands and eruption of continental flood basalts in Ethiopia. Additionally, our data track the influence of geomorphology and local geology on the progressive evolution of the Nile sedimentary signal downstream.

Palaeoproterozoic and Archaean cratons

The Nile traverses Precambrian rocks of the Congo Craton and Saharan Metacraton. The geology of the Saharan Metacraton (Fig. 1) is poorly understood owing to the overlying sedimentary cover and desert sands, and as a result very few modern isotope data are available to help constrain its age and tectonic evolution; the U–Pb ages reported by Abdelsalam *et al.* (2002) are discordant pre-chemical abrasion isotope dilution thermal ionization mass spectrometry ages, or model ages derived by zircon evaporation techniques, which yield poorly constrained $^{207}Pb/^{206}Pb$ ages only. However, Bea *et al.* (2011) reported Archaean U–Pb SHRIMP ages as old as 3 Ga for gneisses at Uweinat, with evidence for crust as old as 3.22 Ga at Gebel Kamil in southern Egypt. Similar ages have been obtained in this study for gneisses from *c.* 80 km east of Uweinat, within the region mapped as the meta-igneous Gebel

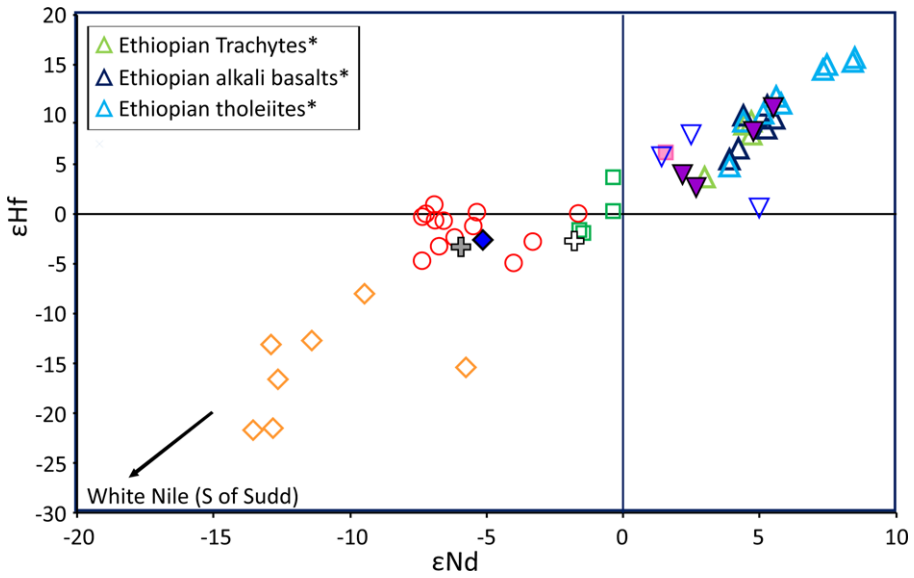

Fig. 10. ε_{Hf} plotted against ε_{Nd} for the same samples as shown in Figure 8. *Ethiopian basalt data from Meshesha & Shinjo (2010). Symbols as in Figure 9, except as noted.

Kamil Series by Bea *et al.* (2011). The sample studied here (WD16A) has evidence for a metasedimentary protolith (broken pre-metamorphic zircon cores), with evidence for zircon growth between *c.* 3.2 and 2.9 Ga, and subsequent metamorphism at *c.* 2.7 Ga. Depleted mantle Hf model ages lie between 3.4 and 3.5 Ga. We see no evidence in our data for the *c.* 2 Ga thermal event (the Eburnean orogeny) recorded by Bea *et al.* (2011).

Sample N7-17S, a modern river sand sample collected at Murchison Falls, Uganda, was sampled from within the NE Congo Block of the Congo Craton, close to the Aswa Shear Zone, which forms the boundary with remobilized crust of the Saharan Metacraton to the north (Appel *et al.* 2005; Katumwehe *et al.* 2016), adjacent to the Pan-African Central African Fold Belt. Zircons from this sample have similar Hf model ages (Fig. 4) to the Archaean gneiss sample from the Saharan Metacraton (WD16A). Zircons in the Murchison Falls sample record crystallization at *c.* 2.7 Ga, *c.* 960 Ma and *c.* 600 Ma; the younger age population forms rims with Hf isotope compositions that are consistent with remelting of similar Archaean crust. The fields defined by the Saharan Metacraton and modern river White Nile provide the best estimate of the composition of Precambrian cratonic basement in the Nile catchment. The 600 Ma zircon rims, and similar aged rutile, plagioclase and mica, indicate penetration of the effects of the Pan-African Orogeny deep into the craton interior, in agreement with the previous work and conclusions of Appel *et al.* (2005) and Schenk *et al.* (2007).

The Hammamat Formation

The depositional and tectonic environment of the Hammamat Formation, which overlies the Precambrian Arabian–Nubian Shield basement, is disputed (e.g. Ries *et al.* 1983; Wilde & Youssef 2002; Abdeen & Greiling 2005; Eliwa *et al.* 2010; Johnson *et al.* 2011; Bezenjani *et al.* 2014). Proposed depositional ages lie close to the time of the Pan-African Orogeny, and both pre-collisional and post-collisional settings have been proposed. Local versus long-distance provenance is debated. Previous work has recorded detrital zircon grains with ages as young as 585 Ma in the Hammamat Formation (Wilde & Youssef 2002), which has implications for assigning a maximum depositional age to these rocks. The volcanic arenite sample from the Hammamat Formation studied here contains four zircon grains that give $^{206}Pb/^{238}U$ ages younger than 620 Ma. In detail, these grains are slightly discordant, and repeat analysis (five analyses for each grain) demonstrated that these grains had indeed undergone Pb loss, and had crystallization ages of 635 – 640 Ma (Fig. 7). This is consistent with the age of the youngest concordant zircon population with consistent hafnium isotope composition in the dataset, of *c.* 640 Ma. In the light of this, we suggest that any maximum depositional ages for the Hammamat Formation based on sparse young grain ages should take into account the possibility that such grains have undergone Pb loss.

Hammamat Formation zircon data analysed as part of this study (Figs 5–7) can be explained by derivation from underlying local Arabian–Nubian Shield bedrock, which is dominated by zircons with juvenile hafnium isotope compositions derived from 870 – 630 Ma oceanic arc rocks (e.g. Stern *et al.* 2010). A small number of pre-Neoproterozoic detrital zircons are found in the Hammamat Formation. Wilde & Youssef (2002) suggested that possible source areas for these pre-Neoproterozoic grains could be the Central and South Eastern Desert, or further afield in the Arabian–Nubian Shield in parts of Saudi Arabia where sparse zircons of this age have previously been recorded. However, we believe that such distal sources are not required to explain our data because it is possible that these zircons have been derived from the more proximal Egyptian Arabian–Nubian Shield (Ali *et al.* 2009). The Arabian–Nubian Shield bedrock in Egypt incorporates some inherited pre-880 Ma igneous zircons with juvenile ε_{Hf} values indicating either incorporation of sediments during subduction along a passive margin or inheritance from the mantle source region, or both (Stern *et al.* 2010).

The volcanic lithic arenite composition and epidote-rich nature of the Hammamat bedrock sample (RSH14A) supports our interpretation that it is derived directly from Arabian–Nubian Shield arc rocks. Furthermore, the composition and zircon U–Pb ages of the sample are in stark contrast to the overlying post-collisional Phanerozoic cover sequences in the region, which are quartz arenites with ZTR values as high as 99 and have diverse zircon U–Pb age spectra, including a typical 600 Ma peak as described below. We therefore see no requirement to invoke long-distance transport of detritus to form the Hammamat Formation.

Phanerozoic sedimentary cover rocks and overlying modern sediment

Our analyses provide the first isotopic data from the Phanerozoic sedimentary cover bedrocks in Egypt. Samples from Phanerozoic sandstone cover sequences in the Western Desert and Red Sea Hills of Egypt are mineralogically mature. They compare well with Phanerozoic cover successions in surrounding regions across North Africa and the Middle East in terms of both zircon age spectra (e.g. compare with data from North Africa; Avigad *et al.* 2003, 2012), and zircon ε_{Hf} characteristics, namely the typical 'double plunge' to negative values at *c.* 600 and *c.* 1000 Ma (e.g. compare with data from Jordan; Morag *et al.* 2011), first recognized as characteristic in Israeli coastal sands by Be'eri-Shlevin *et al.* (2014).

Red Sea Hills Phanerozoic cover rocks and modern wadi samples do not consist entirely of material recycled from the underlying Arabian–Nubian Shield basement. They are derived, at least in part, from areas other than the underlying Arabian–Nubian Shield basement. This is indicated by the following: (1) the occurrence of >2000 Ma zircons, which are extremely rare in the Arabian–Nubian Shield (Stern *et al.* 2010); (2) the increased mineralogical maturity and more complex zircon populations compared with the underlying locally sourced Hammamat Formation (see above); (3) the presence of a significant 1000 Ma population with cratonic ε_{Hf} values, which is incompatible with derivation from the juvenile arc of the Arabian–Nubian Shield.

A similar conclusion was reached by Morag *et al.* (2011), who looked at ε_{Hf} values of the 1000 Ma zircon population in cover sequences of Israel and Jordan. Although their data showed a preponderance of grains with negative ε_{Hf} values, our data from Egypt show two populations at *c.* 1000 Ma, one with positive ε_{Hf} values and one with negative values. Whereas the population with positive values would be compatible with derivation from an as yet unrecorded arc from within the Arabian–Nubian Shield, the provenance of the population with negative ε_{Hf} values remains enigmatic. The cratonic *c.* 1000 Ma zircons found in the Mesozoic cover of both Western Desert and Red Sea Hills samples can be most simply explained by recycling from underlying Palaeozoic cover sequences, but the original basement source is debated. As pointed out by Kolodner *et al.* (2009), long-distance transport from suitable cratonic source areas far to the south are ruled out by the paucity of >2000 Ma grains, which would also be present if derived from such a region. Avigad *et al.* (2003) proposed that the source could be material transported from East Africa towards the margins of Gondwana by Neoproterozoic glaciers. We suggest that the original source may have been from a region since rifted off Gondwana, which may have also supplied zircons to, for example, the Neoproterozoic Arkenu Formation cover sediments of Libya, which contain grains of an appropriate age (Meinhold *et al.* 2011).

Phanerozoic bedrock samples and Red Sea Hills modern wadi sand that partially covers the bedrock have similar zircon U–Pb age

spectra and show a similar 'double plunge' of ε_{Hf} characteristics to negative values at *c.* 600 and *c.* 1000 Ma (Figs 5 and 6). This similarity suggests that the origin of the modern sand is broadly as recycled material from Phanerozoic sedimentary rocks that the sand mantles. Some component of aeolian transport undoubtably contributes in the deposition of such modern sands. However, the extent of such transport distance is difficult to determine given the similarity of Phanerozoic sedimentary cover signature across vast distances of North Africa. Western Desert dune sands were not analysed for zircon U–Pb, and thus an assessment of far-field aeolian input distinct from that recycled from Phanerozoic sandstones cannot be assessed. The similarity in bulk-rock data between the Western Desert mudstone and the aeolian dune sand leads us to tentatively suggest that, as in the Red Sea Hills, composition of the modern sand is broadly similar to Phanerozoic sedimentary bedrock.

Young zircons derived from the Ethiopian Highlands

Cenozoic zircons were found in the Blue Nile (sample ETH2A), the Tekeze and Atbara rivers (ETH6A, ETH8A, SD06) and downstream in the Nile trunk in Sudan (SD04). Grains of such age were not recorded in the White Nile or modern wadi sediment from the Red Sea Hills (Fig. 8). The obvious source for these grains is the Cenozoic Ethiopian volcanic province in the Ethiopian Highlands (Fig. 1), which includes a variety of volcanic units from flood basalts to shield volcanoes, and bimodal compositions with significant ignimbrites and rhyolitic airfall tuffs intercalated with the basalt lava flows (Ukstins *et al.* 2002; Kieffer *et al.* 2004; Prave *et al.* 2016). Our Cenozoic grain ages extend from *c.* 23 to 33 Ma, with population peaks at 25 and 30 Ma. These compare well with the timing of a major period of bimodal and silicic volcanism in Ethiopia, dated at *c.* 25 – 30 Ma (Ukstins *et al.* 2002). Furthermore, Hf analyses that we undertook on both our samples and grains from Lake Tana Rhyolites of the Ethiopian Highlands, previously analysed for U–Pb by Prave *et al.* (2016), show an excellent match (Fig. 8). Ukstins *et al.* (2002) documented pre-rift bimodal magmatism in Ethiopia from 31 to 24 Ma. They recorded a major decrease in volcanism between 25 and 20 Ma, which they associated with the transition from pre- to syn-rift volcanism triggered by the separation of Africa and Arabia. The zircons we have analysed would, by their definition, be of pre-rift origin.

Effects of geomorphology, local bedrock geology and aeolian input on the isotope signal of the Nile River

North of Uganda, the White Nile passes through an extensive area of marshland (the Sudd), which has trapped most of the detritus from the river since 2.7 Ma (Williams & Talbot 2009). This is clearly reflected in the detrital zircon data. Zircons in Ugandan White Nile modern river sediments, south of the Sudd, are dominated by Archaean grains with evidence for crustal reworking and new zircon growth at *c.* 960 and 600 Ma. A craton-dominated signature is also displayed by the highly negative ε_{Nd} values and high $^{87}Sr/^{86}Sr$ values of the White Nile muds.

By contrast, north of the Sudd at Kosti, the detrital signature of White Nile zircons is much less cratonic. In sample SD02A, located north of the Sudd but south of the Gezira Fan, Archaean grains are almost completely absent, and instead the zircon populations show strong similarities to Blue Nile and/or Phanerozoic cover sediment signatures. A mud sample from the same location has Sr–Nd–Hf values similar to those of Phanerozoic cover (Figs 9 and 10). Potential contributing sources to this White Nile sample north of the Sudd could be the Sobat River and/or alluvial fans draining into the river from the Nuba Mountains.

The River Sobat drains similar lithologies to the Blue Nile. Published data show it to have $^{87}Sr/^{86}Sr$ values of 0.708 – 0.712 and ε_{Nd} values of −1.6 to −9.1 (Padoan *et al.* 2011), spanning the range of our data for modern muds from Phanerozoic cover, as sampled in the Red Sea Hills. However, the River Sobat flows through an extensive region of marshland north of the Sudd (the Machar Marshes) and thus was not considered to be a significant source of sediment to the Nile trunk downstream by Padoan *et al.* (2011).

Sample SD02 was collected north of Kosti, close to the southern limit of the Gezira Fan, so significant input of Blue Nile material from the fan is not thought to be likely, and, furthermore, such input would not be compatible with the bulk sediment Sr and Nd data. However, from the Last Glacial Maximum (*c.* 20 ka) onwards, a major alluvial fan (the Khor Abu Habl alluvial fan) has drained into the river from the Nuba Mountains to the west (Williams *et al.* 2000). Ephemeral rivers feeding the fan drain Proterozoic basement rocks and overlying Phanerozoic siliciclastic cover sequences, thus compatible with the isotopic signatures observed in this sample.

Further downstream, a mud sample at SD01B, collected just to the south of Khartoum, has an ε_{Nd} of −1.8 and $^{87}Sr/^{86}Sr$ of 0.7067, a signature with affinity to the Ethiopian Continental Flood Basalts. This is due to the sample location being adjacent to the Gezira Fan (Williams & Talbot 2009), which formed during the Late Pleistocene by overspill from the Blue Nile and contributes today to White Nile sediment load. Significant contribution from the palaeo-Blue Nile sourced Gezira Fan is also reflected in the zircon age spectrum of sample SD01A (Fig. 5) where the dominant peak at 800 Ma strongly resembles the modern Blue Nile signature of sample SD03A in Sudan.

Further downstream to the north, the Blue Nile, and then the Atbara, join the Nile trunk. Both the Blue Nile and the Atbara (with its tributary the Tekeze) drain, from south to north downstream, Cenozoic volcanic rocks, Phanerozoic cover, Arabian–Nubian Shield and Proterozoic basement with Pan-African mineral cooling ages (Mock *et al.* 1999). Sr–Nd–Hf isotope data indicate that the Atbara has a higher proportion of volcanic detrital contribution to the river sediment compared with the Blue Nile. This is also reflected in petrographic data showing a higher proportion of clinopyroxene and olivine (Garzanti *et al.* 2006), and a higher proportion of V and Cr in the Atbara compared with the Blue Nile (Fig. 3). By contrast, a sample collected from a tributary of the Tekeze (the Uri River) in an area of Phanerozoic cover rocks has an isotope composition typical of Phanerozoic cover successions (Figs 9 and 10). Variation in the contributing bedrock lithology is also illustrated by the significant change in proportions of major zircon populations in the Blue Nile downstream. Notably, the region of Arabian–Nubian Shield cut by the Blue Nile in NW Ethiopia contains granitoids with U–Pb zircon ages in the ranges 650 – 700 and 800 – 880 Ma, and juvenile ε_{Nd} values (data summarized by Johnson 2014). These populations are clearly represented in our Blue Nile dataset (Fig. 5), with prominent peaks at 800 – 830 Ma in samples ETH02A and SD03A, persisting into the Nile trunk at Dongola (sample SD04A). Zircons of 680 Ma are also abundant in sample ETH02A from the Blue Nile, and in the southern Nile trunk (SD04A).

The Nile trunk sample downstream of the White Nile confluence with the Blue Nile and Atbara, at Dongola in Sudan (SD04A), shows a U/Pb zircon signature much the same as that of the Atbara and Blue Nile combined. Garzanti *et al.* (2006) suggested a greater input to the trunk Nile from the Blue Nile compared with the Atbara, based on petrographic data. The greater similarity in Sr–Nd and Cr and V values between the Blue Nile and Nile trunk, compared with the Atbara and Nile trunk (Figs 3 and 9), is consistent with this proposal.

By the time the Nile River reaches northern Egypt (sample BS01A; Figs 5 and 6), its signature has changed to more closely

resemble that of typical Phanerozoic sedimentary cover in terms of zircon age spectra, with more Palaeoproterozoic to Archaean grains, and the double plunging ε_{Hf} to negative values at *c.* 600 and *c.* 1000 Ma, also clearly observed in a Nile sample collected near Cairo by Iizuka *et al.* (2013). This downstream change can be explained by the Nile's route in this stretch of the river, which flows across the Phanerozoic sedimentary bedrock cover and overlying modern sediment of the Red Sea Hills to the east and the Western Desert to the west. Any sediment input to the Nile from the west would more likely be transported to the river by aeolian processes, and from the east would include flash flood transportation, given the higher topography of the Red Sea Hills compared with the Western Desert.

Overall, when considering the entire length of the Nile, undoubtably aeolian transportation plays a part in delivering detritus to the river. However, such input does not mask the dominant bedrock and geomorphological controls that we have demonstrated to effect the changes in the river's signature downstream, for both sand and mud grade material.

Finally, we consider that the contribution of the White Nile to the Nile delta is small, the result of both its significantly lower mean annual discharge compared with the Blue Nile and sediment trapping in the Sudd Marshes. Both Sr–Nd and trace element values of the trunk Nile are more similar to those of the Blue Nile–Atbara than to those the White Nile (Figs 3, 9 and 10). Additionally, the white micas of the trunk Nile show similarity in Ar–Ar age distribution to grains collected from the Red Sea Hills, and dissimilarity to the age spectra from the White Nile south of the Sudd. Although pre-Neoproterozoic zircon grains make up to 97% of sediment in the White Nile south of the Sudd, such aged grains in the Nile trunk are not required to be delivered by the White Nile. Pre-Neoproterozoic grains are in fact extremely sparse in the White Nile north of the Sudd (average 2%). Pre-Neoproterozoic grains are relatively common in the Phanerozoic cover sedimentary rocks and modern wadi sediments sampled in the Red Sea Hills (average 9%) and the Western Desert (average 12%), and are also found in the Blue Nile (average 1%) and in sediments from the Atbara and Tekeze (average 6%) (Fig. 5). Any of these regions could have supplied the pre-Neoproterozoic zircons recorded in the Nile trunk.

Supercontinent assembly and the Pan-African Orogeny

Figure 11 shows all of the U/Pb and Hf isotope data derived from Nile hinterland samples as part of this study. The largest peak at *c.* 600 Ma relates to the assembly of East and West Gondwana, when Neoproterozoic juvenile intra-oceanic island arcs of the Arabian–Nubian Shield accreted and finally collided with the Saharan Metacraton and Congo Craton (Johnson *et al.* 2011).

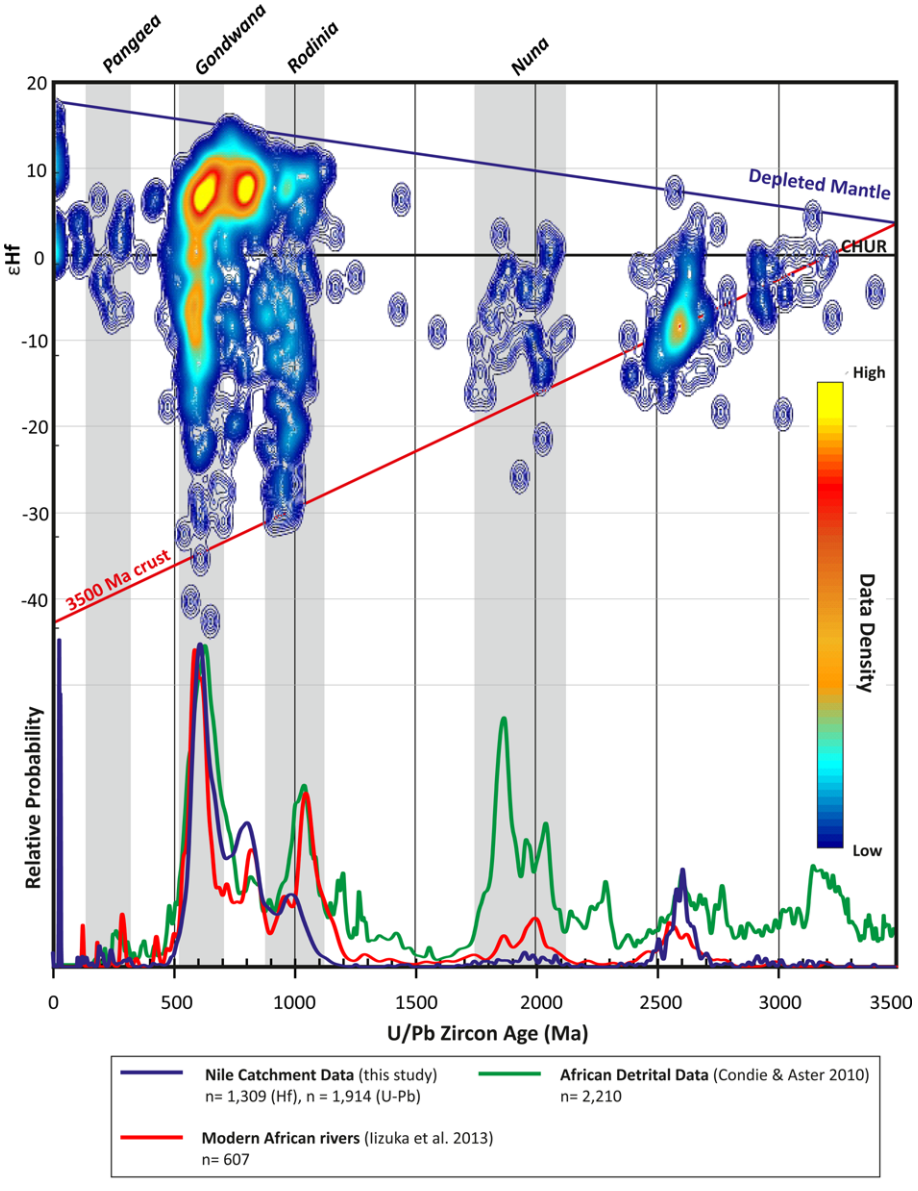

Fig. 11. Probability density plot illustrating the Hf isotope–time evolution of the Nile source regions supplying detrital zircons discussed in this study. The density of the data distribution is calculated using a modified version of the MATLAB implementation of the Kernel Density Estimation procedure supplied by Botev *et al.* (2010) using bandwidths equivalent to the typical analytical uncertainty of the U/Pb ages (±20 Ma) and ε_{Hf} values (±1 epsilon units). Contours are generated by the MATLAB *contour3* function and plotted using the *plot3d* function. Also shown are the compilation of African detrital data from Condie & Aster (2010), and the modern African river data of Iizuka *et al.* (2013) filtered using the discordance criteria applied in this paper.

This can be seen in samples derived from as far afield as the White Nile in Uganda.

The influence of the Pan-African Orogeny is also seen in U/Pb rutile, and Ar/Ar plagioclase and mica ages, which reflect post-orogenic cooling. This is in agreement with hornblende, muscovite, amphibole, biotite and sericite $^{40}Ar/^{39}Ar$ data from Arabian–Nubian Shield bedrock (Johnson *et al.* 2011).

In detail, the zircon U–Pb and Hf-isotope data show two maxima at *c.* 840 – 780 and 700 – 600 Ma with juvenile ε_{Hf} values, which represent two major episodes of arc development within the Arabian–Nubian Shield. The reduction in data density between the two episodes may relate to reduced subduction-related magmatism at this time, perhaps resulting from collisions between arcs within the Arabian–Nubian Shield. Arc collision is documented by the emplacement of ophiolites at this time (Ali *et al.* 2010), and may be represented in our dataset by *c.* 750 Ma detrital zircons from the Hammamat Formation, which have the highest (most juvenile) ε_{Hf} values in the entire dataset.

The final closure of the Mozambique Ocean is documented by the marked switch to more negative ε_{Hf} values in the *c.* 600 Ma population, owing to the intrusion of post-collisional granites derived by melting of continental crust within the suture zone.

A notable feature of the data is the discontinuity of the field of *c.* 1000 Ma grains with juvenile ε_{Hf} versus those with more cratonic influence (i.e. $\varepsilon_{Hf} < 0$). Although the ultimate source of these grains remains unknown, our data suggest two distinct ultimate sources, one from an oceanic-arc setting and a second involving remelting of a cratonic source.

The most cratonic (i.e. lowest ε_{Hf}) grains within each age population in our dataset plot close to the 3500 Ma evolution line for North African crust derived using our basement data from the Saharan Metacraton in Egypt and Congo Craton in Uganda.

The supercontinent cycles that led to the creation of Gondwana (650 – 500 Ma) are represented in all of the samples collected as part of this study (Fig. 11). The isotope signatures of the samples analysed from the Nile River and its hinterland contain Mesoproterozoic and older zircons that may be related to earlier supercontinent cycles. However, the location of the Congo Craton in reconstructions of Rodinia (De Waele *et al.* 2008) is a matter of debate and the lack of exposure and reliable geological data from the Saharan Metacraton means that its location in Rodinia and earlier supercontinent configurations is unknown. Although our data contain some *c.* 2000 Ma zircons, these cannot be directly related to the formation of the supercontinent 'Nuna' (aka Colombia) because Nuna did not involve North African cratons (Rogers & Santosh 2002).

Conclusions

Gneissic basement of the Saharan Metacraton in southern Egypt and detrital zircons derived from rocks of the Congo Craton in northern Uganda both indicate an age of crust formation between 3.0 and 3.5 Ga, with subsequent melting and/or metamorphism at *c.* 2.7 Ga.

Our combined U–Pb and Hf isotope zircon dataset documents the evolution of the North African crust, in particular highlighting phases in the development of the Arabian–Nubian Shield and its collision with the Saharan Metacraton. The data show two phases of arc magmatism, at *c.* 840 – 780 and 700 – 600 Ma, with a reduction in magmatism at *c.* 750 Ma, during a period of arc collisions within the Arabian–Nubian Shield.

The Hammamat Formation, sampled in Wadi Hammamat, has a maximum depositional age of 635 Ma, based on reanalysis of anomalously young zircon grains, which are shown to have undergone Pb loss. Provenance analysis indicates that the Hammamat Formation is locally derived. By contrast, the Phanerozoic cover sedimentary rocks overlying the Arabian–Nubian Shield are derived, at least in part, from distal sources beyond the Arabian–Nubian Shield. Phanerozoic cover sedimentary rocks that blanket much of NE Africa represent an important source of detritus to the Nile River and are characterized by the presence of a major zircon population with both juvenile and crustal ε_{Hf} values reflecting the Pan-African orogenic event, and a significant (9 – 12%) population of pre-Neoproterozoic zircon grains. The original source of *c.* 1000 Ma grains in the Phanerozoic sedimentary cover rocks remains enigmatic, but we have identified that there are two distinct populations: one indicating a juvenile ultimate source and one a cratonic source.

In the modern Nile drainage, there is considerable evolution downstream, controlled predominantly by changes in local geology and geomorphology. The provenance signature of the White Nile is dramatically different upstream and downstream of the Sudd marshes as a result of sediment trapping. South of the Sudd, White Nile sediments are craton-derived. North of the Sudd, at Kosti, the signature of the White Nile is dominated by material derived from Phanerozoic sandstones supplied via alluvial fans to the west of the river. Further north, south of Khartoum, White Nile sediment composition is affected by its proximity to the Pleistocene Blue Nile sourced Gezira Fan. The Blue Nile's and Atbara's signatures are influenced predominantly by input from the Ethiopian flood basalts in terms of their bulk-rock signature, and by proximity to the Arabian–Nubian Shield in terms of zircon characteristics. A further shift in sediment signature in terms of zircon characteristics is seen by the time the Nile reaches northern Egypt, reflecting the passage of this stretch of the river through Phanerozoic cover sedimentary rocks and overlying modern sands of the Red Sea Hills and Western Desert. By contrast, the bulk isotopic Sr–Nd–Hf data show little downstream evolution and remain dominated by mafic input from the Ethiopian Highlands as far south as northern Egypt.

Acknowledgements and Funding

This work was funded by an NERC Open CASE PhD studentship award NE/I018433/1, BP Egypt and awards from the NERC Isotope Geoscience Facilities Steering Committee (IP-1248-0511, IP-1299-0512). We gratefully acknowledge the expertise of F. Darius at the Freie Universität, Berlin, Germany, and M. Abo Elwfa Muhammad for our Egyptian fieldwork, T. Berhanu of Addis Ababa University in Ethiopia, and M. Ibrahim and family, along with our guides Midhat and Moez in Sudan. At NIGL, we thank C. Stewart, V. Pashley and N. Roberts for valuable laboratory assistance. This paper benefited from careful reviews by W. Bosworth and R. Stern.

Scientific editing by Peter Clift

References

Abdeen, M.M. & Greiling, R.O. 2005. A quantitative structural study of Late Pan-African compresssional deformation in the Central Eastern Desert (Egypt) during Gondwana assembly. *Gondwana Research*, **8**, 457–471.

Abdelsalam, M.G., Liégeois, J.-P. & Stern, R.J. 2002. The Saharan Metacraton. *Journal of African Earth Sciences*, **34**, 119–136.

Abdelsalam, M.G., Gao, S.S. & Liégeois, J.-P. 2011. Upper mantle structure of the Saharan Metacraton. *Journal of African Earth Sciences*, **60**, 328–336.

Ali, B.H., Wilde, S.A. & Gabr, M.M.A. 2009. Granitoid evolution in Sinai, Egypt, based on precise SHRIMP U–Pb zircon geochronology. *Gondwana Research*, **15**, 38–48.

Ali, K.A., Azer, M.K., Gahlan, H.A., Wilde, S.A., Samuel, M.D. & Stern, R.J. 2010. Age constraints on the formation and emplacement of Neoproterozoic ophiolites along the Allaqi–Heiani Suture, South Eastern Desert of Egypt. *Gondwana Research*, **18**, 583–595.

al-Miṣrīyah, H. 1981. *Geologic map of Egypt*. Egyptian Geological Survey and Mining Authority, Cairo.

Altumi, M.M., Elicki, O., Linnemann, U., Hofmann, M., Sagawe, A. & Gärtner, A. 2013. U–Pb LA-ICP-MS detrital zircon ages from the Cambrian of Al Qarqaf Arch, central–western Libya: Provenance of the West Gondwanan sand sea at the dawn of the early Palaeozoic. *Journal of African Earth Sciences*, **79**, 74–97.

Andresen, A., El-Rus, M.A.A., Myhre, P.I., Boghdady, G.Y. & Corfu, F. 2009. U–Pb TIMS age constraints on the evolution of the Neoproterozoic Meatiq Gneiss Dome, Eastern Desert, Egypt. *International Journal of Earth Sciences*, **98**, 481–497.

Appel, P., Schenk, V. & Schumann, A. 2005. *PT* path and metamorphic ages of pelitic schists at Murchison Falls, NW Uganda Evidence for a Pan-African tectonometamorphic event in the Congo Craton. *European Journal of Mineralogy*, **17**, 655–664.

Avigad, D., Kolodner, K., McWilliams, M., Persing, H. & Weissbrod, T. 2003. Origin of northern Gondwana Cambrian sandstone revealed by detrital zircon SHRIMP dating. *Geology*, **31**, 227–230.

Avigad, D., Gerdes, A., Morag, N. & Bechstädt, T. 2012. Coupled U–Pb–Hf of detrital zircons of Cambrian sandstones from Morocco and Sardinia: Implications for provenance and Precambrian crustal evolution of North Africa. *Gondwana Research*, **21**, 690–703.

Baker, J., Thirlwall, M. & Menzies, M. 1996. Sr–Nd–Pb isotopic and trace element evidence for crustal contamination of plume-derived flood basalts: Oligocene flood volcanism in western Yemen. *Geochimica et Cosmochimica Acta*, **60**, 2559–2581.

Bea, F., Montero, P., Anbar, M.A. & Talavera, C. 2011. SHRIMP dating and Nd isotope geology of the Archean terranes of the Uweinat–Kamil inlier, Egypt–Sudan–Libya. *Precambrian Research*, **189**, 328–346.

Be'eri-Shlevin, Y., Avigad, D., Gerdes, A. & Zlatkin, O. 2014. Detrital zircon U–Pb–Hf systematics of Israeli coastal sands: new perspectives on the provenance of Nile sediments. *Journal of the Geological Society, London*, **171**, 107–116, http://doi.org/10.1144/jgs2012-151

Bezenjani, N.R., Pease, V., Whitehouse, M.J., Shalaby, M.H., Kadi, K.A. & Kozdroj, W. 2014. Detrital zircon geochronology and provenance of the Neoproterozoic Hammamat Group (Igla Basin), Egypt and the Thalbah Group, NW Saudi Arabia: Implications for regional collision tectonics. *Precambrian Research*, **245**, 225–243.

Bosworth, W., Huchon, P. & McClay, K. 2005. The Red Sea and Gulf of Aden Basins. *Journal of African Earth Sciences*, **43**, 334–378.

Bosworth, W., El-Hawat, A.S., Helgeson, D.E. & Burke, K. 2008. Cyrenaican 'shock absorber' and associated inversion strain shadow in the collision zone of northeast Africa. *Geology*, **36**, 695–698.

Botev, Z.I., Grotowski, J.F. & Kroese, D.P. 2010. Kernel density estimation via diffusion. *Annals of Statistics*, **38**, 2916–2957.

Breitkreuz, C., Eliwa, H. *et al.* 2010. Neoproterozoic SHRIMP U–Pb zircon ages of silica-rich Dokhan Volcanics in the North Eastern Desert, Egypt. *Precambrian Research*, **182**, 163–174.

Buck, W. 2006. The role of magma in the development of the Afro-Arabian Rift System. *In*: Yirgu, G., Ebinger, C.J. & Maguire, P.K.H. (eds) *The Afar Volcanic Province within the East African Rift System*. Geological Society, London, Special Publications, **259**, 43–54, http://doi.org/10.1144/GSL.SP.2006.259.01.05

Cahen, L., Snelling, N.J., Delhal, J.V. & Vail, J.R. 1984. *The Geochronology and Evolution of Africa*. Clarendon Press, Oxford.

Condie, K.C. & Aster, R.C. 2010. Episodic zircon age spectra of orogenic granitoids: The supercontinent connection and continental growth. *Precambrian Research*, **180**, 227–236.

Daumain, G., Dubertret, L. & Lelubre, M. 1958. *Esquisse Structurale Provisoire de l'Afrique*. Documents Originaux Services Géologiques. Association des Services Géologiques Africains (ASGA) Congrès Géologique International, Paris.

De Waele, B., Johnson, S. & Pisarevsky, S. 2008. Palaeoproterozoic to Neoproterozoic growth and evolution of the eastern Congo Craton: its role in the Rodinia puzzle. *Precambrian Research*, **160**, 127–141.

Ebinger, C. 2005. Continental break-up: the East African perspective. *Astronomy and Geophysics*, **46**, 2.16–2.21.

Eliwa, H., Breitkreuz, C., Khalaf, I. & Gameel, K.E. 2010. Depositional styles of Early Ediacaran terrestrial volcanosedimentary succession in Gebel El Urf area, North Eastern Desert, Egypt. *Journal of African Earth Sciences*, **57**, 328–344.

El-Rahman, Y.A., Polat, A., Fryer, B.J., Dilek, Y., El-Sharkawy, M. & Sakran, S. 2010. The provenance and tectonic setting of the Neoproterozoic Um Hassa Greywacke Member, Wadi Hammamat area, Egypt: Evidence from petrography and geochemistry. *Journal of African Earth Sciences*, **58**, 185–196.

Evuk, D., Franz, G., Frei, D. & Lucassen, F. 2014. The Neoproterozoic evolution of the central–eastern Bayuda Desert (Sudan). *Precambrian Research*, **240**, 108–125.

Flowerdew, M., Millar, I., Vaughan, A., Horstwood, M. & Fanning, C. 2006. The source of granitic gneisses and migmatites in the Antarctic Peninsula: a combined U–Pb SHRIMP and laser ablation Hf isotope study of complex zircons. *Contributions to Mineralogy and Petrology*, **151**, 751–768.

Gani, N.D.S., Gani, M.R. & Abdelsalam, M.G. 2007. Blue Nile incision on the Ethiopian Plateau: Pulsed plateau growth, Pliocene uplift, and hominin evolution. *GSA Today*, **17**, 4–11.

Gani, N.D., Abdelsalam, M.G., Gera, S. & Gani, M.R. 2009. Stratigraphic and structural evolution of the Blue Nile Basin, Northwestern Ethiopian Plateau. *Geological Journal*, **44**, 30–56.

Garzanti, E. & Andò, S. 2007. Heavy mineral concentration in modern sands: implications for provenance interpretation. *Developments in Sedimentology*, **58**, 517–545.

Garzanti, E., Andò, S., Vezzoli, G., Ali Abdel Megid, A. & El Kammar, A. 2006. Petrology of Nile River sands (Ethiopia and Sudan): Sediment budgets and erosion patterns. *Earth and Planetary Science Letters*, **252**, 327–341.

Garzanti, E., Padoan, M., Setti, M., Najman, Y., Peruta, L. & Villa, I.M. 2013. Weathering geochemistry and Sr–Nd fingerprints of equatorial upper Nile and Congo muds. *Geochemistry, Geophysics, Geosystems*, **14**, 292–316.

Garzanti, E., Ando, S., Padoan, M., Vezzoli, G. & El Kammar, A. 2015. The modern Nile sediment system: Processes and products. *Quaternary Science Reviews*, **130**, 9–56.

Ghebreab, W. 1998. Tectonics of the Red Sea region assessed. *Earth-Science Review*, **45**, 1–44.

Goodwin, A.M. 1996. *Principles of Precambrian Geology*. Academic Press, New York.

Guiraud, R., Bosworth, W., Thierry, J. & Delplanque, A. 2005. Phanerozoic geological evolution of Northern and Central Africa: An overview. *Journal of African Earth Sciences*, **43**, 83–143.

Iizuka, T., Campbell, I.H., Allen, C.M., Gill, J.B., Maruyama, S. & Makoka, F. 2013. Evolution of the African continental crust as recorded by U–Pb, Lu–Hf and O isotopes in detrital zircons from modern rivers. *Geochimica et Cosmochimica Acta*, **107**, 96–120.

Issawi, B. & McCauley, J.F. 1992. The Cenozoic rivers of Egypt, the Nile problem. *In*: Adams, B. & Friedman, R. (eds) *The Followers of Horus, studies dedicated to Michael Allen Hoffman 1944–1990*. Oxbow Press, Oxford, 1–18.

Johnson, P.R. 2014. An expanding Arabian–Nubian Shield geochronologic and isotopic dataset: defining limits and confirming the tectonic setting of a Neoproterozoic accretionary orogen. *Open Geology Journal*, **8**, 3–33.

Johnson, P.R. & Woldehaimanot, B. 2003. Development of the Arabian–Nubian Shield: perspectives on accretion and deformation in the northern East African Orogen and the assembly of Gondwana. *In*: Yoshida, M., Windley, B.E. & Dasgupta, S. (eds) *Proterozoic East Gondwana: Supercontinent Assembly and Breakup*. Geological Society, London, Special Publications, **206**, 289–325, http://doi.org/10.1144/GSL.SP.2003.206.01.15

Johnson, P.R., Andresen, A. *et al.* 2011. Late Cryogenian–Ediacaran history of the Arabian–Nubian Shield: A review of depositional, plutonic, structural, and tectonic events in the closing stages of the northern East African Orogen. *Journal of African Earth Sciences*, **61**, 167–232.

Katumwehe, A.B., Abdelsalam, M.G., Atekwana, E.A. & Laó-Dávila, D.A. 2016. Extent, kinematics and tectonic origin of the Precambrian Aswa Shear Zone in eastern Africa. *Gondwana Research*, **34**, 241–253.

Kazmin, V. 1972. *Geological map of Ethiopia*. Geological Survey of Ethiopia, Ministry of Mines, Energy and Water Resources, Addis Ababa.

Kenea, N.H., Ebinger, C.J. & Rex, D.C. 2001. Late Oligocene volcanism and extension in the southern Red Sea Hills, Sudan. *Journal of the Geological Society, London*, **158**, 285–294, http://doi.org/10.1144/jgs.158.2.285

Kieffer, B., Arndt, N. *et al.* 2004. Flood and shield basalts from Ethiopia: magmas from the African superswell. *Journal of Petrology*, **45**, 793–834.

Klitzsch, E.H. & Squyres, C.H. 1990. Paleozoic and Mesozoic geological history of north eastern Africa based upon new interpretation of Nubian strata. *AAPG Bulletin*, **74**, 1203–1211.

Kolodner, K., Avigad, D., McWilliams, M., Wooden, J.L., Weissbrod, T. & Feinstein, S. 2006. Provenance of north Gondwana Cambrian–Ordovician sandstone: U–Pb SHRIMP dating of detrital zircons from Israel and Jordan. *Geological Magazine*, **143**, 367–391.

Kolodner, K., Avigad, D., Ireland, T.R. & Garfunkel, Z. 2009. Origin of Lower Cretaceous ('Nubian') sandstones of North-east Africa and Arabia from detrital zircon U–Pb SHRIMP dating. *Sedimentology*, **56**, 2010–2023.

Krom, M.D., Stanley, J.D., Cliff, R.A. & Woodward, J.C. 2002. Nile River sediment fluctuations over the past 7000 yr and their key role in sapropel development. *Geology*, **30**, 71–74.

Kusky, T.M. & Matsah, M.I. 2003. Neoproterozoic dextral faulting on the Najd fault system, Saudi Arabia, preceded sinistral faulting and escape tectonics related to closure of the Mozambique Ocean. *In*: Yoshida, M., Windley, B.E. & Dasgupta, S. (eds) *Proterozoic East Gondwana: Supercontinent Assembly and Breakup*. Geological Society, London, Special Publications, **206**, 327–361, http://doi.org/10.1144/GSL.SP.2003.206.01.16

Macgregor, D.S. 2012. The development of the Nile drainage system: integration of onshore and offshore evidence. *Petroleum Geoscience*, **18**, 417–431, http://doi.org/10.1144/petgeo2011-074

Mark, D., Barfod, D., Stuart, F. & Imlach, J. 2009. The ARGUS multicollector noble gas mass spectrometer: Performance for $^{40}Ar/^{39}Ar$ geochronology. *Geochemistry, Geophysics, Geosystems*, **10**, Q0AA02, http://doi.org/10.1029/2009GC002643.

McLennan, S. & Taylor, S. 1985. *The Continental Crust: Its Composition and Evolution: An Examination of the Geochemical Record Preserved in Sedimentary Rocks*. Blackwell Scientific, Oxford.

Meinhold, G., Morton, A.C. *et al.* 2011. Evidence from detrital zircons for recycling of Mesoproterozoic and Neoproterozoic crust recorded in Paleozoic and Mesozoic sandstones of southern Libya. *Earth and Planetary Science Letters*, **312**, 164–175.

Meinhold, G., Morton, A.C. & Avigad, D. 2013. New insights into peri-Gondwana paleogeography and the Gondwana super-fan system from detrital zircon U–Pb ages. *Gondwana Research*, **23**, 661–665.

Meshesha, D. & Shinjo, R. 2010. Hafnium isotope variations in Bure volcanic rocks from the northwestern Ethiopian volcanic province: a new insight for mantle source diversity. *Journal of Mineralogical and Petrological Sciences*, **105**, 101–111.

Ministry of Energy and Mines 1981. *Geological Map of the Sudan*. Geological and Mineral Resources Department, Khartoum.

Mock, C., Arnaud, N.O., Cantagrel, J.-M. & Yirgu, G. 1999. $^{40}Ar/^{39}Ar$ thermochronology of the Ethiopian and Yemeni basements: reheating related to the Afar plume? *Tectonophysics*, **314**, 351–372.

Morag, N., Avigad, D., Gerdes, A., Belousova, E. & Harlavan, Y. 2011. Detrital zircon Hf isotopic composition indicates long-distance transport of North Gondwana Cambrian–Ordovician sandstones. *Geology*, **39**, 955–958.

Omar, G.I. & Steckler, M.S. 1995. Fission track evidence on the initial rifting of the Red Sea: two pulses, no propagation. *Science*, **270**, 1341–1344.

Padoan, M., Garzanti, E., Harlavan, Y. & Villa, I.M. 2011. Tracing Nile sediment sources by Sr and Nd isotope signatures (Uganda, Ethiopia, Sudan). *Geochimica et Cosmochimica Acta*, **75**, 3627–3644.

Palacios, Z.H. 2013. Climate change as a controlling parameter in sediment supply: the Nile Province. University of Aberdeen. http://ethos.bl.uk/OrderDetails.do?uin=uk.bl.ethos.575393#sthash.0i0YHMsQ.dpuf

Pik, R., Deniel, C., Coulon, C., Yirgu, G., Hofmann, C. & Ayalew, D. 1998. The northwestern Ethiopian Plateau flood basalts: classification and spatial distribution of magma types. *Journal of Volcanology and Geothermal Research*, **81**, 91–111.

Pik, R., Deniel, C., Coulon, C., Yirgu, G. & Marty, B. 1999. Isotopic and trace element signatures of Ethiopian flood basalts: evidence for plume–lithosphere interactions. *Geochimica et Cosmochimica Acta*, **63**, 2263–2279.

Pik, R., Marty, B., Carignan, J. & Lavé, J. 2003. Stability of the Upper Nile drainage network (Ethiopia) deduced from (U–Th)/He thermochronometry: implications for uplift and erosion of the Afar plume dome. *Earth and Planetary Science Letters*, **215**, 73–88.

Prave, A.R., Bates, C.R., Donaldson, C.H., Tolland, H., Condon, D.J., Mark, D. & Raub, T.D. 2016. Geology and geochronology of the Tana Basin, Ethiopia: LIP volcanism, super eruptions, and Eocene–Oligocene environmental change. *Earth and Planetary Science Letters*, **443**, 1–8.

Revel, M., Colin, C. *et al.* 2014. 21,000 years of Ethiopian African monsoon variability recorded in sediments of the western Nile deep-sea fan. *Regional Environmental Change*, **14**, 1685–1696.

Ries, A.C., Shackleton, R.M., Graham, R.H. & Fitches, W.R. 1983. Pan-African structures, ophiolites and mélange in the Eastem Desert of Egypt: a traverse at 26°N. *Journal of the Geological Society, London*, **140**, 20, http://doi.org/10.1144/gsjgs.140.1.0075

Rochette, P., Tamrat, E. *et al.* 1998. Magnetostratigraphy and timing of the Oligocene Ethiopian traps. *Earth and Planetary Science Letters*, **164**, 497–510.

Rogers, J.J. & Santosh, M. 2002. Configuration of Columbia, a Mesoproterozoic supercontinent. *Gondwana Research*, **5**, 5–22.

Schenk, V., Appel, P., Jons, N., Loose, D., Schumann, A. & Wegner, H. 2007. Metamorphic reworking of the Congo craton in Uganda. *Geochimica et Cosmochimica Acta*, **71**, A887.

Shukri, N.M. 1949. The mineralogy of some Nile sediments. *Quarterly Journal of the Geological Society of London*, **106**, 466–467, http://doi.org/10.1144/GSL.JGS.1949.105.01-04.19

Sparks, R.S.J., Folks, C.B., *et al.* 2008. Uturuncu volcano, Bolivia: Volcanic unrest due to mid-crustal magma intrusion. *American Journal of Science*, **308**, 727–769.

Squire, R.J., Campbell, I.H., Allen, C.M. & Wilson, C.J.L. 2006. Did the Transgondwanan Supermountain trigger the explosive radiation of animals on Earth? *Earth and Planetary Science Letters*, **250**, 116–133.

Stern, R.J. 1994. Arc-assembly and continental collision in the Neoproterozoic African orogen: implications for the consolidation of Gondwanaland. *Annual Review of Earth and Planetary Sciences*, **22**, 319–351.

Stern, R.J. & Hedge, C.E. 1985. Geochronologic and isotopic constraints on late Precambrian crustal evolution in the eastern desert of Egypt. *American Journal of Science*, **285**, 97–127.

Stern, R.J., Ali, K.A., Liegeois, J.P., Johnson, P.R., Kozdroj, W. & Kattan, F.H. 2010. Distribution and significance of Pre-Neoproterozoic zircons in juvenile Neoproterozoic igneous rocks of the Arabian Nubian Shield. *American Journal of Science*, **310**, 791–811.

Tadesse, S., Milesi, J.-P. & Deschamps, Y. 2003. Geology and mineral potential of Ethiopia: a note on geology and mineral map of Ethiopia. *Journal of African Earth Sciences*, **36**, 273–313.

Talbot, M.R., Williams, M.A.J. & Adamson, D.A. 2000. Strontium isotope evidence for late Pleistocene reestablishment of an integrated Nile drainage network. *Geology*, **28**, 343–346.

Tchameni, R., Mezger, K., Nsifa, N. & Pouclet, A. 2000. Neoarchaean crustal evolution in the Congo Craton: evidence from K-rich granitoids of the Ntem Complex, southern Cameroon. *Journal of African Earth Sciences*, **30**, 133–147.

Ukstins, I.A., Renne, P.R., Wolfenden, E., Baker, J., Ayelew, D. & Menzies, M. 2002. Matching conjugate volcanic rifted margins: $^{40}Ar/^{39}Ar$ chrono-stratigraphy of pre- and syn-rift bimodal flood volcanism in Ethiopia and Yemen. *Earth and Planetary Science Letters*, **198**, 289–306.

Walraven, F. & Rumvegeri, B. 1993. Implications of whole-rock Pb–Pb and zircon evaporation dates for the early metamorphic history of the Kasaï craton, Southern Zaïre. *Journal of African Earth Sciences*, **16**, 395–404.

Wilde, S. & Youssef, K. 2002. A re-evaluation of the origin and setting of the Late Precambrian Hammamat Group based on SHRIMP U–Pb dating of detrital zircons from Gebel Umm Tawat, North Eastern Desert, Egypt. *Journal of the Geological Society, London*, **159**, 595–604, http://doi.org/10.1144/0016-764901-081

Williams, M.A. & Adamson, D.A. 1982. *A Land between Two Niles*. Balkema, Rotterdam.

Williams, M.A. & Talbot, M.R. 2009. Late Quaternary environments in the Nile Basin. *In*: Dumont, H.J. (ed.) *The Nile: Origin, Environments, Limnology and Human Use*. Springer, Berlin, 61–72.

Williams, M.A.J., Adamson, D., Cock, B. & McEvedy, R. 2000. Late Quaternary environments in the White Nile region, Sudan. *Global and Planetary Change*, **26**, 305–316.

Williams, M.A.J., Adamson, D., Prescott, J.R. & Williams, F.M. 2003. New light on the age of the White Nile. *Geology*, **31**, 1001–1004.

Willis, K.M., Stern, R.J. & Clauer, N. 1988. Age and geochemistry of late Precambrian sediments of the Hammamat series from the Northeastern desert of Egypt. *Precambrian Research*, **42**, 173–187.

Woodward, J., Macklin, M. *et al.* 2015. Shifting sediment sources in the world's longest river: A strontium isotope record for the Holocene Nile. *Quaternary Science Reviews*, **130**, 124–140.